Palaeogeography, Palaeoclimatology, Palaeoecology 555 (2020) 109824

Contents lists available at ScienceDirect

Palaeogeography, Palaeoclimatology, Palaeoecology

journal homepage: www.elsevier.com/locate/palaeo

Biogeochemical evidence from OGCP Core 2A sediments for environmental changes preceding deposition of Tuff IB and climatic transitions in Upper Bed I of the Olduvai Basin

Andrea M. Shilling[a,*], Devon E. Colcord[a], Jonathan Karty[b], Angela Hansen[b], Katherine H. Freeman[c], Jackson K. Njau[a,d], Ian G. Stanistreet[d,e], Harald Stollhofen[f], Kathy D. Schick[d,g], Nicholas Toth[d,g], Simon C. Brassell[a,*]

[a] Department of Earth and Atmospheric Sciences, Indiana University, Bloomington, IN, USA
[b] Department of Chemistry, Indiana University, Bloomington, IN, USA
[c] Department of Geosciences, The Pennsylvania State University, University Park, PA, USA
[d] The Stone Age Institute, Gosport, IN, USA
[e] Department of Earth, Ocean, and Ecological Sciences, University of Liverpool, Liverpool, UK
[f] GeoZentrum Nordbayern, Fredrich-Alexander-Universität (FAU), Erlangen, Germany
[g] Department of Anthropology, Indiana University, Bloomington, IN, USA

ARTICLE INFO

Keywords:
EARS
Tanzania
Biomarkers
n-alkanes
Paleoclimate

ABSTRACT

Sediment cores recovered by the Olduvai Gorge Coring Project (OGCP) in 2014 afford the opportunity to examine the coupling of biogeochemical evidence for climatic and environmental change within the context of hominin evolution at this renowned East African locality. Investigations of elemental (total organic carbon – TOC or C_{org} wt%, carbon to nitrogen ratio - C/N), molecular (source-specific biomarkers), and isotopic ($\delta^{13}C_{org}$, $\delta^{2}H_{nC31}$) compositions of organic matter provide evidence for temporal changes in sedimentary materials derived from terrestrial plants (C_3, C_4) and aquatic producers (algae, sponges, cyanobacteria), and in precipitation. The 13 kyr record of Upper Bed I immediately preceding Tuff IB extends high-resolution stratigraphic profiles of precession-scale alternations of wetter and drier conditions to encompass the entire interval from the Bed I Basalt to Tuff IB. The second wetter interval, designated W2, records local influences on climate and water supply consistent with evidence for discrete sediment sources based its physical properties (e.g., gamma radiation, magnetic susceptibility) compared with the overall sequence. The $\delta^{13}C_{TOC}$ values for wetter interval W2 reveal two millennial-scale (~2.5 kyr) drier episodes followed by a shift in the dominance of C_3 over C_4 plants accompanying the transition to a drier climate (D3). Moreover, biogeochemical data for Upper Bed I show that changes from drier to wetter conditions occur more rapidly (~900 yr) than wetter to drier transitions (>2.6 kyr), based on interpolated ages. In addition, biomarker profiles indicate that aquatic plants, primarily algae and macrophytes, may have been subject to more profound and faster fluctuations than variations in terrestrial vegetation expressed in terms of the relative proportions of woodland and grassland settings. Thus, environmental and climatic changes not only influenced the availability of resources of food and shelter for hominins within the Olduvai region but also led to their variation on centennial to millennial to precessional timescales.

1. Introduction

Extensive research on the ~2 Myr sequence of fluvial-lacustrine and volcanic deposits at Olduvai Gorge, Tanzania, has enhanced understanding of hominin evolution through discovery of numerous fossil and archaeological finds (e.g., Leakey, 1971) from outcrops and trenches that provide their sedimentological context (e.g., Hay, 1976; Ashley and Hay, 2002; deMenocal, 2004; Trauth et al., 2005; Trauth et al., 2007; Maslin et al., 2014). Developments in early hominin evolution have been postulated to correspond with changes in climate

* Corresponding author.
E-mail addresses: andshill@indiana.edu (A.M. Shilling), jkarty@indiana.edu (J. Karty), asorg@indiana.edu (A. Hansen), khf4@psu.edu (K.H. Freeman), jknjau@indiana.edu (J.K. Njau), harald.stollhofen@fau.de (H. Stollhofen), kaschick@indiana.edu (K.D. Schick), toth@indiana.edu (N. Toth), simon@indiana.edu (S.C. Brassell).

https://doi.org/10.1016/j.palaeo.2020.109824
Received 17 April 2019; Received in revised form 25 May 2020; Accepted 27 May 2020
Available online 05 June 2020

(Dart, 1925; Vrba, 1995; Potts, 1998; deMenocal, 2011; Donges et al., 2011), including the marked changes in hominin diversity observed during the critical interval of ~2.0 to 1.7 Ma during the early Pleistocene (Shultz et al., 2012; Shultz and Maslin, 2013; Maslin et al., 2014; Maxwell et al., 2018). Globally, this time interval corresponds to the strengthening of the climatic coupling of ocean and atmosphere known as the Walker Circulation (Ravelo et al., 2004; McClymont and Rosell-Melé, 2005; Ravelo, 2006), although there is evidence to suggest that equatorial regions may have experienced zonal circulation prior to this time (Etourneau et al., 2010; Zhang et al., 2014). The resultant changes in precipitation and temperature in East Africa led to an episode of large lake formation (Trauth et al., 2007; Shultz and Maslin, 2013) and directly influenced the climate and landscape experienced by hominins (Trauth et al., 2005; Trauth et al., 2007; Maslin et al., 2014). Indeed, the ~300 kyr interval from ~2.0 to 1.7 Ma is associated with substantive, global-scale climatic changes that are contemporaneous with critical hominin evolutionary events in East Africa, including early hominin migration (Agusti and Lordkipanidze, 2011; Antón et al., 2014; Maslin et al., 2014), peak species diversity (Trauth et al., 2007; Shultz et al., 2012; Shultz and Maslin, 2013; Maslin et al., 2014; Bobe and Carvalho, 2019), and the advent of a marked increase in cranial capacity (Shultz et al., 2012; Shultz and Maslin, 2013;). Hence, investigations of East African paleoclimate records seek to determine whether climate change serves as a driver for hominin evolution (deMenocal, 1995, 2011; Shultz et al., 2012; Potts, 2013; Antón et al., 2014; Maslin et al., 2014, 2015). These research endeavors benefit from enhanced understanding of both the paleo-landscape that hominins encountered and its rate of change, although the ability to establish the role of climate in hominin evolution may currently be limited by the fossil record (Maxwell et al., 2018). The sedimentary record of Olduvai Gorge have served as the basis for many efforts to reconstruct depositional paleoenvironments because several horizons within these strata can be directly associated with hominin activity (Ashley et al., 2010a, 2010b; Barboni et al., 2010; Albert and Bamford, 2012; Bennett et al., 2012; Stanistreet, 2012; Blumenschine et al., 2012; Magill et al., 2016; Aramendi et al., 2017; Albert et al., 2018; Stanistreet et al., 2018a, 2018b). Studies at Olduvai Gorge have typically focused on examination of samples and data garnered from outcrops in the gorge and/or from trenches dug into its walls, which have the benefit of allowing assessment of the nature and extent of lateral variation in sedimentology at each individual site. The presence of diagnostic, dated marker beds, especially tuffs (Deino, 2012; McHenry, 2012), recognized at a substantive number and range of locations within Olduvai Gorge has enabled stratigraphic correlation across many sites that help place fossil evidence of hominins, their activities (Bunn et al., 1986; Blumenschine, 1995; Blumenschine et al., 2012; Arráiz et al., 2017) and likely diets (Cerling et al., 2011) within a well-defined temporal context. Yet, outcrop and trench materials collected at or near the surface typically has limitations for biogeochemical investigations because of their exposure to prolonged weathering, which tends to degrade organic matter (OM), compromising its preservation and limiting the ability to assess its more labile characteristics (Canuel and Martens, 1996; Schouten et al., 2010).

A key stratigraphic unit in Olduvai Gorge that contains many archaeological and vertebrate fossil assemblages is the Bed I Upper Member sensu Hay (1976). Upper Bed I deposits are bracketed by the Bed I Basalt and Tuff IF that have previously been dated based on outcrop samples, respectively, to 1.877 ± 0.013 Ma and 1.803 ± 0.002 Ma (Deino, 2012) and therefore span ~74 kyr of the Pleistocene. The presence of other dated horizons within Upper Bed I, notably Tuff IB (1.848 ± 0.003 Ma; Deino, 2012), further aids correlation between sites, complementing use of numerous, characteristic fossil assemblages and marker beds (Barboni et al., 2010; Albert and Bamford, 2012; Blumenschine et al., 2012; Stanistreet, 2012; Blumenschine et al., 2012b; Magill et al., 2016; Aramendi et al., 2017; Albert et al., 2018; Stanistreet et al., 2018a) that collectively help characterize the lacustrine sedimentary sequence of Olduvai Gorge. The timing for deposition of Upper Bed I also corresponds with the presence of an ephemeral deep lake at Olduvai, which existed from 1.84 to 1.74 Ma (Ashley and Hay, 20022), concurrent with the occurrence of large lakes elsewhere in East Africa (Trauth et al., 2007; Maslin and Christensen, 2007; Shultz and Maslin, 2013).

Biogeochemical investigations of samples from Upper Bed I outcrops have identified the types of vegetation represented in the paleoenvironment and shown that their temporal variations can be coupled to precession-scale changes in climate (Magill et al., 2013a, 2013b). They have also provided evidence helpful in defining the characteristics of the Olduvai paleo-landscapes that early hominins would have encountered and the plant resources they afforded (Ashley et al., 2010a; Albert et al., 2015; Albert et al., 2018), including interpretations of the types of vegetation and plant species associated with hominin activities (Magill et al., 2016). These studies have all relied on sediment samples obtained from outcrops or trenches where evaluation of biogeochemical proxies tends to be limited to refractory components, such as plant wax *n*-alkanes (Magill et al., 2013a, 2013b; Driese and Ashley, 2016; Dominguez-Rodrigo et al., 2017), that best survive exposure and weathering. However, even the most robust proxies can be compromised by losses associated with OM preservation, the extent of bacterial degradation, and the effect of physical weathering processes, which means that increased amounts of material are required to compensate for lower concentrations of target compounds. One significant outcome of this approach is that it decreases the temporal resolution attainable and thereby limits the ability to determine the rates of change in paleoenvironment and climate. In effect, development of high-resolution stratigraphic records of proxies based on labile biomarkers that are prone to oxidative degradation and/or components that tend to occur in low concentrations requires access to sediment sequences in a better state of preservation than those typically encountered in outcrops and trenches. Thus, the well-preserved sedimentary OM in cores recovered by the Olduvai Gorge Coring Project (OGCP) in 2014, especially OGCP Core 2A that targeted the Paleolake Olduvai depocenter during Bed I times, represents a depositional sequence well-suited for extensive, high-resolution biomarker analyses (Colcord et al., 2018, 2019; Shilling et al., 2019).

Prior biogeochemical investigations of Upper Bed I sediments from OGCP Core 2A have revealed: (i) precession-scale variations in $\delta^{13}C_{org}$ resembling those observed in outcrop (Magill et al., 2013a, 2013b) accompanied by evidence for shorter-term fluctuations (Colcord et al., 2018), (ii) temporal variations in the abundances of specific aquatic and terrestrial biomarkers associated with the alternating wetter and drier intervals that are characterized by variations in $\delta^{13}C_{org}$ and $\delta^{2}H_{nC31}$ (Colcord et al., 2019), and (iii) a stark decrease in OM and biomarker preservation associated with changes in the depositional setting of Paleolake Olduvai after deposition of Tuff IB that appears to reflect its transition to a shallower, perennial lake (Shilling et al., 2019).

This study complements and extends the prior work on OGCP Core 2A by examining sedimentological, isotopic, and molecular evidence contained within the well-preserved sediment sequence from Paleolake Olduvai preceding deposition of Tuff IB. It determines the changes in vegetation and aquatic productivity during this interval associated with a transition from wetter to drier conditions and integrates these data with those of each wetter and drier intervals within the Upper Bed I sequence to assess whether there are indications of climate-driven variations or temporal trends in the sources of OM and environmental proxies that are distinct from the signals associated with precession-driven changes in precipitation. It also specifically examines both isotopic and molecular signals recording biological responses to the transitions from wetter to drier conditions and vice versa, especially the signatures of terrestrial and aquatic biomarkers, in an effort to constrain the comparative timescales of these environmental changes. This approach offers the potential to discern how local influences in the hydrology of the Olduvai basin may have influenced the sediment record

of precession-scale variations in precipitation, and affords the possibility of recognizing evidence for other (non-Milankovitch) cyclical patterns of changes in climate.

In summary, the principal objectives of this study are to elucidate stratigraphic variations in isotopic and molecular signals, notably for biomarkers diagnostic for aquatic biota and terrestrial vegetation, within Upper Bed I. These data are then considered within their sedimentological framework to assess how temporal variations in the Olduvai paleoenvironment, especially environmental responses to the transition between wetter and drier intervals and evidence for sub-Milankovitch variability (cf. Colcord et al., 2018), potentially reflect the effects of local hydrologic changes. In addition, the centennial-scale resolution (cf. Donges et al., 2011) of the biogeochemical signatures from OGCP Core 2A should enable determination of temporal constraints on the rate of changes in the paleoenvironment and climate of Olduvai that may have influenced hominin evolution.

2. Olduvai Gorge: background and sediment cores

2.1. Setting of study site

Olduvai Gorge lies adjacent to the eastern branch of the East African Rift System (EARS) in northern Tanzania (Fig. 1). It exposes Pleistocene fan-deltaic and fluvio-lacustrine outcrops that span ~2 Myr (Hay, 1976) and include volcanic materials sourced from the Ngorongoro Volcanic Highlands to the east. Among the volcanoes within the Ngorongoro Volcanic Highlands, Olmoti is identified as the likely source of the Upper Bed I tuffs that occur in Olduvai Gorge (Mollel and Swisher, 2012; McHenry, 2012). Geochemical fingerprinting of tuffs and basalt aid correlations between stratigraphic units within the gorge (Stollhofen et al., 2008; McHenry, 2012; Habermann et al., 2016) and, most recently, helped to establish the temporal alignment of the OGCP core sequences with those within the gorge succession (McHenry et al., 2019).

The occurrence of laminated lacustrine deposits at Locality 80 (Hay, 1976; Hay and Kyser, 2001; Fig. 1) with lake margin deposits to the east and west helped establish the position of the central basin of Paleolake Olduvai during deposition of Bed I. At this time the lake was broad, shallow, largely closed hydrologically, and saline-alkaline (Hay, 1976; Hay and Kyser, 2001; Sikes and Ashley, 2007; Stollhofen et al., 2008; Bamford et al., 2008; Barboni et al., 2010; Deocampo et al., 2017) and varied in its extent (Sikes and Ashley, 2007; Stollhofen et al., 2008; Stanistreet, 2012; Beverly et al., 2014; Stanistreet et al., 2018a). Horizons between the Bed I Basalt and Tuff IB have been the focus of numerous paleoanthropological studies, notably those at the DK locale (Leakey, 1969Leakey et al., 1971; Stanistreet et al., 2018a), which has been characterized as a wetland environment (Albert et al., 2015) with evidence for hominin activities represented by stone tools and butchered faunal remains (Potts, 1984; Reti, 2016).

Rainfall in the Olduvai area was high (~800 mmyr^{-1}) during the wetter intervals of Bed I deposition (Sikes and Ashley, 2007; Magill et al., 2013a). Yet the elevation of the Ngorongoro Volcanic Highlands – and therefore their rain shadow – plus the tropical rainbelt (formerly called the ITCZ) and the Congo Air Boundary (CAB) would also have influenced precipitation, which controls the weather regime of Olduvai Gorge and its seasonal cycle, given that its latitude (~3°S) limits temperature variability (Speth and Davis, 1976; Nicholson, 2000). Present-day rainy seasons in the Olduvai region (Magill et al., 2013b) consist of long rains from the northeasterly monsoon (March to May) and short rains from the southeasterly monsoon (October to December), which may have been more important during deposition of Upper Bed I (Deocampo et al., 2017). In addition, changes in the position of volcanic highlands from Ngorongoro at 2.0 Ma to Olmoti at 1.85 Ma may have affected the rain shadow affecting the Paleolake Olduvai area (Stanistreet et al., 2020b).

2.2. Core sampling

In 2014, ~245 m of sediment core, with ~94% recovery, was collected by OGCP from Borehole 2A (02° 58′ 43.0″ S, 035° 19′ 25.5″ E; Fig. 1), a site chosen to target the thickest Upper Bed I sequence associated with the likely depocenter of Paleolake Olduvai. Care was taken to avoid contamination by lubricants and other petroleum products both during and after drilling. Once recovered, each section of core was tubed, sealed, and shipped to the National Lacustrine Core Facility (LacCore) at the University of Minnesota for sampling and storage. After each core was split, two separate sets of samples were taken at approximately every 16 cm from the center of the core – to minimize potential contamination from core sidewalls – throughout the Upper Bed I section of Core 2A. Smaller samples (<1 g) were collected for bulk geochemical analyses and larger (<20 g) samples spanning 3 cm were taken for detailed biomarker analyses.

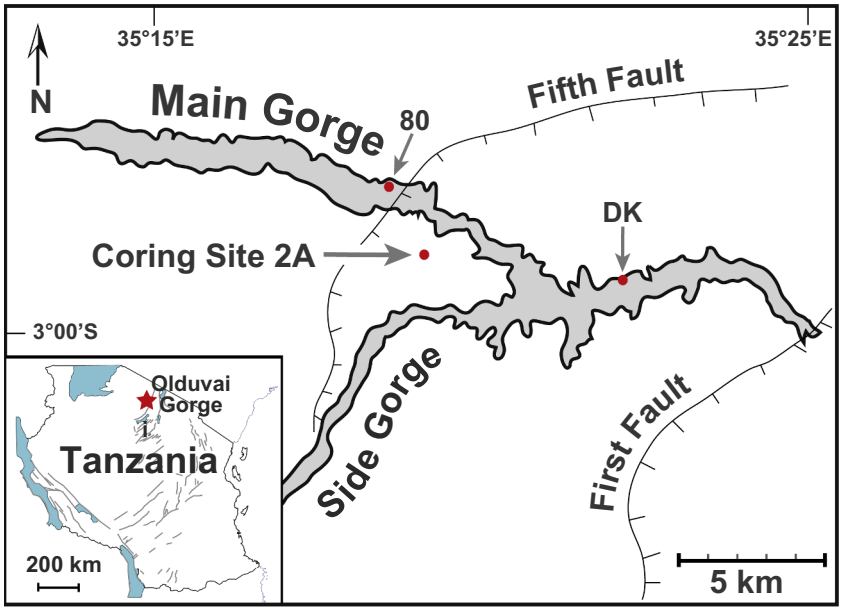

Fig. 1. Map of Tanzania (insert) showing the location of Olduvai Gorge in relation to major faults of the EARS and present-day lakes combined with expanded map of Olduvai Gorge indicating the location of OGCP Borehole 2A, local major faults, and the 80 and DK geological and fossil localities. (Adapted from Colcord et al., 2018.)

2.3. Physical properties

An integral part of the initial description of OGCP Core 2A included use of a Geotek Multi Sensor Core Logger-S to obtain core logs for gamma density, P-wave velocity, magnetic susceptibility (loop), non-contact resistivity, natural gamma radiation, and spectrophotometry, with a spatial resolution ranging from 0.5 to 4 cm, depending on the property measured. Once split, the colour reflectance and point magnetic susceptibility were measured at 0.5 cm resolution on the archived half of OGCP Core 2A using a Geotek Multi Sensor Core Logger-XYZ, and core photographs were taken with a Geotek Core Imaging System (CIS), yielding images with a resolution of 200 pixelscm^{-1}. This study includes use of point source magnetic susceptibility (SI x 10^{-5}) and natural gamma radiation (CPS) data for OGCP Core 2A, which were measured every 0.5 cm and 3.8 cm, respectively. These two sets of data, provided by LacCore (National Lacustrine Core Facility, Department of Earth Sciences, University of Minnesota – Twin Cities), quantify variations in composition throughout the core expressed in terms of the proportion of clay versus sand within the sediments and the relative amounts of magnetic components based on the natural gamma radiation levels and point source magnetic susceptibility.

2.4. Chronology

Three key, dated (Deino, 2012), marker beds (Bed I Basalt, Tuff IB, and Tuff IF) known from outcrops (Hay, 1976; Stollhofen et al., 2008; McHenry, 2012; Habermann et al., 2016) were identified in OGCP Core 2A based on lithostratigraphic correlations (Stanistreet et al., 2020a) supported by geochemical fingerprinting (McHenry et al., 2020a). Our biogeochemical studies (Colcord et al., 2018, 2019; Shilling et al., 2019) focus primarily on the section of core between the Bed I Basalt at 90 m and Tuff IB and ~72 m. Previous dating of these two horizons yielded ages of 1.877 ± 0.013 Ma and 1.848 ± 0.003 Ma, respectively (Deino, 2012), although evidence from precessional cycle periodicity suggests that the Bed I basalt may be older (~1.94 Ma; Stanistreet et al., 2020b). New data establishing the chronology for OGCP Core 2A (Deino et al., 2020) confirms the age of Tuff IB (1.8479 ± 0.0027) but yields a greater age for the Bed I basalt (1.900 ± 0.015 Ma). Linear interpolation between the two dated horizons therefore corresponds to a sediment accumulation rate of ~0.35 mmyr^{-1} rather than the ~0.62 mmyr^{-1} previously employed (Colcord et al., 2018, 2019; Shilling et al., 2019) Thus, sediment sampling at ~16 cm intervals corresponds to a resolution of ~460 yr, with each 3 cm sample representing an integrated signal representing ~90 yr of deposition. However, recognition of desiccation cracks at several horizons within the stratigraphic section (Colcord et al., 2018; Shilling et al., 2019), although more pronounced higher in the section accompanying Tuff IA (Stanistreet et al., 2020a), confirms the presence of hiatuses and confirms that the interpolated sediment accumulation rate represents a minimum value. In parts of the sedimentary sequence (e.g. Core 34Y-2 at ~83.5 m) there are several intervals with individual discrete laminations of sub-millimeter thickness, consistent with the possibility that this layering may represent an annual depositional cycle.

3. Analytical methods and approach

3.1. Bulk sediment geochemistry

Sediment samples (<1 g) were stored frozen after sampling and freeze-dried prior to carbonate dissolution by treatment with excess 1 N HCl. Each sample was rinsed to neutral pH after dissolution was complete and then again freeze-dried. Organic carbon contents (C_{org} as wt %) and the carbon isotopic composition of bulk OM ($\delta^{13}C_{org}$) were measured (typically in duplicate, occasionally in triplicate with an average standard deviation of 0.255) using elemental analysis – isotope ratio mass spectrometry (EA-IRMS) at Indiana University's Stable Isotope Research Facility (SIRF; Colcord et al., 2018). Normalization of $\delta^{13}C_{org}$ values to the Vienna Peedee Belemnite (VPDB) standard employed acetanilide (−29.53‰ ± 0.01) and ethylenediamine tetraacetic acid (EDTA; −40.38‰ ± 0.01) standards provided by Dr. A. Schimmelmann (Indiana University).

3.2. Biomarker protocols

25 samples (<20 g per sample) from the ~4 m segment of Core 2A (72.2–76.4 m depth) were selected for biomarker analyses, complementing the data for 58 samples from the underlying ~10 m (76.6–86.9 m depth; Colcord et al., 2018, 2019). Analytical procedures for biomarker extraction, separation, and analysis followed published methods (Shilling et al., 2019), utilizing dichloromethane/methanol (9:1 v/v) for extraction using an Automated Solvent Extractor (ASE). Each resultant total lipid extract (TLE) was fractionated by sequential column chromatography using silica gel followed by alumina to obtain apolar (hydrocarbon) and ketone fractions after recombination of eluates (cf. Shilling et al., 2019, supplementary material). The apolar and ketone fractions were dried under N_2 and dissolved in hexane (0.25 to 1 ml dependent on C_{org} (wt%) contents (cf. Shilling et al., 2019). Biomarker analysis employed a gas chromatograph - quadrupole time-of-flight mass spectrometer (GC-QTOF-MS) at Indiana University's Mass Spectrometry Facility. Quantifications utilized a squalane standard provided by Dr. A. Schimmelmann (Indiana University). The detection limit for all biomarker measurements was determined as 0.01 μg/gC_{org}. Single GC–MS analyses of each hydrocarbon fraction ensured sufficient material was available to determine δ^2H_{nC31} values utilizing established procedures (Colcord et al., 2018). These isotopic analyses employed a Trace Ultra GC configured via GC-TC to a Delta Plus XP isotope ratio mass spectrometer, normalizing measured δ^2H_{nC31} values to the Vienna Standard Mean Ocean Water (VSMOW) standard using a mixture of *n*-alkanes. The $H3^+$ factor was monitored and fell within the range of 5.6 to 7.6 ppm mV^{-1}.

3.3. Biogeochemical proxies

The analytical approach targeted determination of the occurrence, abundance, and isotopic signatures of specific biomarkers in lacustrine sediments because they can record the response of organisms to paleoclimate and paleoenvironment change that are quantifiable using a series of proxies (Table 1). As examples, the $\delta^{13}C$ and δ^2H compositions of *n*-alkanes afford evidence of dominant vegetation types and precipitation, respectively (Chikaraishi and Naraoka, 2003; Sachse et al., 2004; Feakins and Sessions, 2010), and have helped elucidate both the precipitation history (δ^2H_{nC31}) and temporal changes in terrestrial vegetation ($\delta^{13}C_{n\text{-}C31}$, $\delta^{13}C_{Corg}$, $n\text{-}C_{33}/n\text{-}C_{31}$) of Paleolake Olduvai using samples from outcrops (Magill et al., 2013a, 2013b) and OGCP Core 2A (Colcord et al., 2018, 2019; Shilling et al., 2019). This approach has been complemented by investigation of biomarkers derived from aquatic organisms (Colcord et al., 2019; Shilling et al., 2019), such as alkenones, which are diagnostic of contributions of OM from haptophyte algae (Marlowe et al., 1984; Toney et al., 2012; Nakamura et al., 2014; Randlett et al., 2014; Araie et al., 2018). Thus, collective information from biogeochemical proxies helps decipher both the characteristics of surrounding terrestrial vegetation and aquatic organisms within the lake environment and can establish constraints on the properties of the lake waters (e.g. salinity, oxygen levels; Castañeda and Schouten, 2011), whereas stratigraphic variations in such proxies provide evidence for temporal changes in climate and environment.

Table 1
Biomarkers Origins and Diagnostic Indices.

Compound class	Origins (biological/diagenetic)	References
C_{27}, C_{29}, C_{31}, C_{33} *n*-Alkanes	Plant waxes (trees, grasses)	Eglinton and Hamilton, 1963
C_{17}, C_{19} *n*-Alkanes	Cyanobacteria (and algae)	Brassell et al., 1978; Gelpi et al., 1970; Cranwell et al., 1987; Meyers, 2003; Longman and Palmer, 1987; Ward, 2006
C_{14}, C_{16}, C_{18}, C_{20} *n*-Alkanes	Bacteria (as biosynthetic or degradation products)	Brassell et al., 1978
Fern-8-ene	Ferns (including other fernene isomers)	Ageta et al., 1968; Ageta and Arai, 1983; Brassell and Eglinton, 1984
	Anaerobic bacteria	Brassell et al., 1980, 1981; Volkman et al., 1986; Zhang et al., 2011
Alkenones	Lacustrine haptophytes divide into Group I and II phylotypes based on composition of C_{38} alken-2-ones	Longo et al., 2016, Longo et al., 2018; D'Andrea et al., 2016Nagashima et al., 2018
Steradienes	Dehydration products of sterols from algae, such as haptophytes or diatoms; markers for algal productivity.	Cornford et al., 1979; Mackenzie et al., 1982; Brassell and Eglinton, 1983; McEvoy and Maxwell, 1983; Farrimond et al., 1986; Kennedy and Brassell, 1992; Volkman et al., 1986, Volkman, 2003; Dumitrescu and Brassell, 2005; Rampen et al., 2010
A-norsteranes	Sponges (derived from A-norsterols)	van Grass et al., 1982; Bohlin et al., 1982; Brassell et al., 1983; Volkman, 1988
Phytane	From phytol (chlorophyll side chain) or bacterial phytanyl moieties; prominent in microbial mats	Philp et al., 1978; Didyk et al., 1978; Grossi et al., 1998; Schouten et al., 2001; Fourcans et al., 2004; Hebting et al., 2006; Rontani and Bonin, 2011

Biomarker index	Name, formula, significance	References
C/N atomic ratio	Values reflect relative proportions of terrigenous vs. aquatic OM; higher values indicate more terrigenous OM and lower values indicate more aquatic OM	Meyers and Ishiwatari, 1993
TAR	Terrestrial vs. aquatic ratio = (n-C_{27} + n-C_{29} + n-C_{31})/(n-C_{17} + n-C_{19} + n-C_{21}) higher values = more terrigenous OM, lower values = stronger aquatic influence	Meyers and Ishiwatari, 1993; Bourbonniere and Meyers, 1996; Castañeda and Schouten, 2011
P_{alg}	(n-C_{17} + n-C_{19})/(n-C_{17} + n-C_{19} + n-C_{29} + n-C_{31}), higher values indicate higher proportion of algal sourced *n*-alkanes relative to those from terrestrial vegetation.	Magill et al., 2013a
P_{aq}	(n-C_{23} + n-C_{25})/(n-C_{23} + n-C_{25} + n-C_{29} + n-C_{31}), higher values indicate higher proportion of *n*-alkanes from aquatic macrophytes relative to those from terrestrial vegetation.	Ficken et al., 2000; Magill et al., 2013a
C_{33}/C_{31}	n-C_{33}/n-C_{31}, higher values tend to reflect increased contributions from grasses	Bush and McInerney, 2013; Colcord et al., 2018, 2019
ΣC_{29} + C_{31} + C_{33}	n-C_{29} + n-C_{31} + n-C_{33}, higher concentrations reflect increased plant wax contributions	Bush and McInerney, 2013
Terrestrial vegetation	(n-C_{27} + n-C_{29} + n-C_{31} + n-C_{33}), prominent *n*-alkanes in plant waxes	Shilling et al., 2019
Aquatic Production	(n-C_{17} + n-C_{19} + n-C_{21} + n-C_{23}), derived from algae, cyanobacteria, and macrophytes (C_{23})	Shilling et al., 2019
Microbial Influence	(n-C_{16} + n-C_{18} + n-C_{20} + n-C_{22}), *n*-alkanes reflecting bacterial activity and degradation	Shilling et al., 2019
$U^{K'}_{37}$	C_{37} alkenone unsaturation index [$C_{37:2}$]/([$C_{37:2}$] + [$C_{37:3}$]) values increase with growth temperature of haptophyte producers	Brassell et al., 1986; Prahl et al., 1988
$U^{K'}_{38}$	C_{38} alkenone unsaturation index [$C_{38:2}$]/([$C_{38:2}$] + [$C_{38:3}$]), values increase with growth temperature of haptophyte producers	Pearson et al., 2008
TriMe/diMe MTTCs	Ratio of 5,7,8-trimethyl to 5,7-dimethyl 2-methyl-2-(4,8,12-trimethyltridecyl)chroman, which is a measure of salinity.	Sinninghe Damsté et al., 1987

4. Results

4.1. Core 2A section preceding Tuff IB

4.1.1. Core description and age

The ~4 m of OGCP Core 2A from ~72–76.5 m is comprised primarily of claystones and sandy claystones (Fig. 2) that range in colour from dark brown/black to grey/tan. The lithologic characteristics are comparable to those of the underlying stratigraphic section (76.6–86.9 m; Colcord et al., 2018) except that laminations are absent, which contrasts with the sedimentary sequence deposited during the underlying wetter interval (W1; Colcord et al., 2018). There is evidence for considerable bioturbation in the ~74.5 to 75.5 m core interval, which is comprised of many individual layered horizons, including a thin marlstone (Fig. 2). In addition, XRD analyses reveal that part of the overlying interval (73.44–74.24 m) is dolomite-rich in contrast to the surrounding intervals, which are also carbonate-rich but dominated by calcite (McHenry et al., 2020a, 2020b), mirroring the sediment lithology found at other sites in the Olduvai basin, including Locality 80 (Fig. 1; Hay and Kyser, 2001). There are a few horizons with root traces higher in the stratigraphic section, but none were identified or recognized below ~75.5 m (Fig. 2). Such evidence for discontinuous sedimentation notwithstanding, the accumulation rate of ~0.35 mmyr^{-1} for Upper Bed I based on linear interpolation between the dated horizon of Tuff IB at 72 m (1.8479 ± 0.0027 Ma; Deino et al., 2020) and the Bed I basalt at 90 m (1.900 ± 0.015 Ma; Deino et al., 2020) suggests that the ~72–76.5 m interval corresponds to ~13 kyr.

4.1.2. Isotopic and elemental analyses

The bulk $\delta^{13}C_{org}$ values differ markedly in the ~72 to 76.5 m interval of OGCP Core 2A, with values for the subsections below and above 74.5 m differing by >6‰ (Fig. 3A). Prior assessments of the factors governing $\delta^{13}C_{org}$ in Olduvai Gorge (Magill et al., 2013a, 2013b; Colcord et al., 2018) suggest that sediments deposited below 74.5 m with $\delta^{13}C_{org}$ values generally < −20‰ likely reflect vegetation with a higher proportion of C_3 plants (primarily trees and shrubs) compared with the subsequent interval where $\delta^{13}C_{org}$ values uniformly > −20‰ indicate prominent contributions from C_4 plants (e.g., grasses, other drought-resistant plants, sedges). Thus, the trend in $\delta^{13}C_{org}$ is consistent with the evidence from sedimentology that there is a transition from a wetter to a subsequent drier interval at ~74.5 m (Supplementary Table 1), hereafter described as W2 and D3, respectively (following the designations in Colcord et al., 2018, 2019). In addition, the W2 section exhibits considerable variation in its $\delta^{13}C_{org}$, with samples from 76.1 to 75.3 m depth yielding values similar to those in D3. This isotope excursion event (designated E2) resembles the pattern previously reported for a lower subsection of Core 2A (77.8–78.6 m) where $\delta^{13}C_{org}$ values also exhibit a marked positive excursion event (hereafter E1) during a wetter interval (W2; Colcord et al., 2018). C_{org} contents are lower during the E2 excursion event (Fig. 3B) but otherwise broadly similar for the W2 and D3 sections (averaging 1.75% and 1.78%, respectively; Fig. 3B). The depth profile of the C/N ratio is comparable to that of C_{org} (Fig. 3B), with similar averages for W2 and D3, although the range of C/N values also shows greater variability within W2. The hydrogen isotopic composition of the C_{31} *n*-alkane, $\delta^{2}H_{nC31}$, shows an

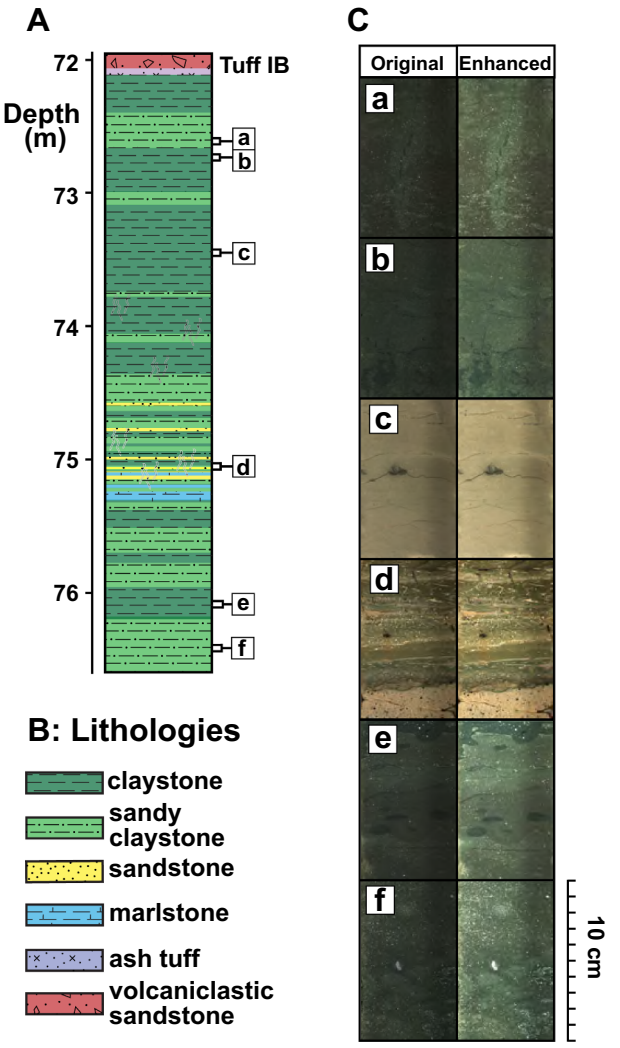

Fig. 2. Stratigraphic column for the 72.2–76.4 m depth section of OGCP Core 2A (A; modified from Shilling et al., 2019) showing major lithologies (B) and a selection of core photos (C; enhanced images have increased brightness and contrast) that provide representative examples of the various sediment lithologies within this interval. a: silty claystone (31Y-1A 49–59 cm). b: claystone (31Y-1A 60–70 cm). c: claystone (31Y-1A 141–151 cm). d: siltstone/sandstone (32Y-1A 17–27 cm). e: claystone (32Y-1A 93–103 cm). f: silty claystone (32Y-1A 135–145 cm).

enrichment of ~5‰ in W2 (average −138.2‰) compared to D3 (average −133.9‰; Fig. 3C), which is consistent with previous interpretations of enriched δ^2H_{nC31} values, corresponding to more arid conditions at Olduvai (Magill et al., 2013b; Colcord et al., 2018). However, the overall range of δ^2H_{nC31} values and their variability is markedly greater in W2; indeed, the highest and lowest values for this entire ~4.5 m section occur only one sample apart. Such marked fluctuations in δ^2H_{nC31} values are perhaps a function of the layered sedimentology (Fig. 2) and attributable to variations in the amount and sources of terrestrial detritus, and its associated OM, entering the depositional regime.

4.1.3. Biomarker records

n-Alkane distributions provide evidence for the source(s) of sedimentary OM that can be expressed using various proxies. The Terrigenous-Aquatic Ratio (TAR; Table 1; Fig. 3D) records higher values representing a stronger terrestrial signal in W2 followed by a decrease in both the average value and their range in D3, which is consistent with a transition to more pronounced aquatic sources of OM. A similar trend is evident in the stratigraphic profiles of the P_{alg} and P_{aq} ratios (Table 1; cf. Magill et al., 2013a; Fig. 3E; Supplementary Table 1) that show increased proportions of *n*-alkanes derived from algal and aquatic macrophytes (Ficken et al., 2000; Magill et al., 2013a: Table 1) within D3. The P_{aq} ratio also increases during the positive isotope excursion event E2 suggesting that the lake margins may have experienced changes during this interval, perhaps an expansion of wetland habitats with emergent macrophytes as the lake level subsided. The C_{33}/C_{31} *n*-alkane ratio (Fig. 3F), primarily a measure of the proportion of grasses in the environment (Table 1; Bush and McInerney, 2013), fluctuates during both wetter and drier intervals likely reflecting differences in the sources of terrestrial OM associated with changes in drainage patterns or increased variability among discrete sources of vegetation, perhaps linked to fire frequency. However, the fact that the profile for $\Sigma C_{29} + C_{31} + C_{33}$ *n*-alkanes (Fig. 3F), which represents a measure of the magnitude of plant wax inputs, is broadly similar to C_{33}/C_{31} suggests that the primary driver for variations in these indices is the supply of terrestrial OM to the lake.

The allochthonous signature is much stronger within D3 as concentrations of biomarkers sourced by aquatic organisms (i.e., phytane, *n*-C_{17}, A-norsteranes, steradienes, and alkenones) all increase markedly within D3 (Fig. 4; Table 1; Supplementary Table 1). Among these components, the concentration ranges and averages of biomarkers derived from bacteria/cyanobacteria (phytane and *n*-C_{17}; Fig. 4F) are an order of magnitude higher in D3 compared with W2. Similarly, alkenones, steradienes, and A-norsteranes are all present in lower concentrations in W2, as seen in their range of values and averages (Fig. 4C, E), although the differences in their abundance between the wetter and drier intervals are less pronounced than those for phytane and *n*-C_{17}, and the timing of the transition is not synchronous with other proxies (Supplementary Table 1). The unsaturation ratios for C_{37} and C_{38} alkenones ($U^{K'}_{37}$ and $U^{K'}_{38}$, respectively; Table 1; Fig. 4D) show marked differences in W2 but more conformable values in D3. Their unsaturation ratios and their depth trends show similarities to those observed in the underlying section of Upper Bed I and perhaps reflect changes in alkenone producers associated with wetter versus drier intervals of the sedimentary record of Paleolake Olduvai.

Among aquatic biomarkers only the A-norsteranes show marked changes in concentration during the excursion in $\delta^{13}C_{org}$ values (event E2), although there is also a slight increase in the abundance of steradienes (Fig. 4E). These increases in steroidal components are consistent with the possibility that the E2 event may reflect changes in lake margins, including expansion of wetland habitats that are conducive to sponges. In addition, the sediment lithology varies toward the end of the W2 interval, consisting of a sequence of thinly layered claystones, silty claystones, and sandstones (Fig. 2). Thus, differences in sedimentology may account for the variability in the concentrations of aquatic biomarkers (alkenones, A-norsteranes, and steradienes; Fig. 4).

Presenting the *n*-alkane distributions as a ternary diagram (Fig. 5) affords further discrimination of the sources of OM because it incorporates assessment of microbial influences of their composition in addition to contributions from terrestrial vegetation and aquatic producers. This approach reveals that the majority of samples from W2 consists of 40 to 70% terrestrially sourced, odd-numbered, long-chain *n*-alkanes, with a few horizons, notably sandier intervals, affording evidence for greater bacterial influence based on their compositions with >50% even-numbered, short-chain *n*-alkanes. The *n*-alkane distributions from D3 reflect a combination of terrestrial vegetation and varying amounts of odd, short- to mid-chain-length *n*-alkanes derived from aquatic producers that become the dominant components in some samples. Thus, the factors controlling *n*-alkane compositions during W2 and D3 are distinctly different. The major variable in the wetter interval appears to be microbial overprinting of the contributions from terrestrial vegetation, especially during the isotope excursion event (E2), which likely reflects a decrease in the supply of plant waxes when precipitation and runoff declined. In contrast, the drier interval is

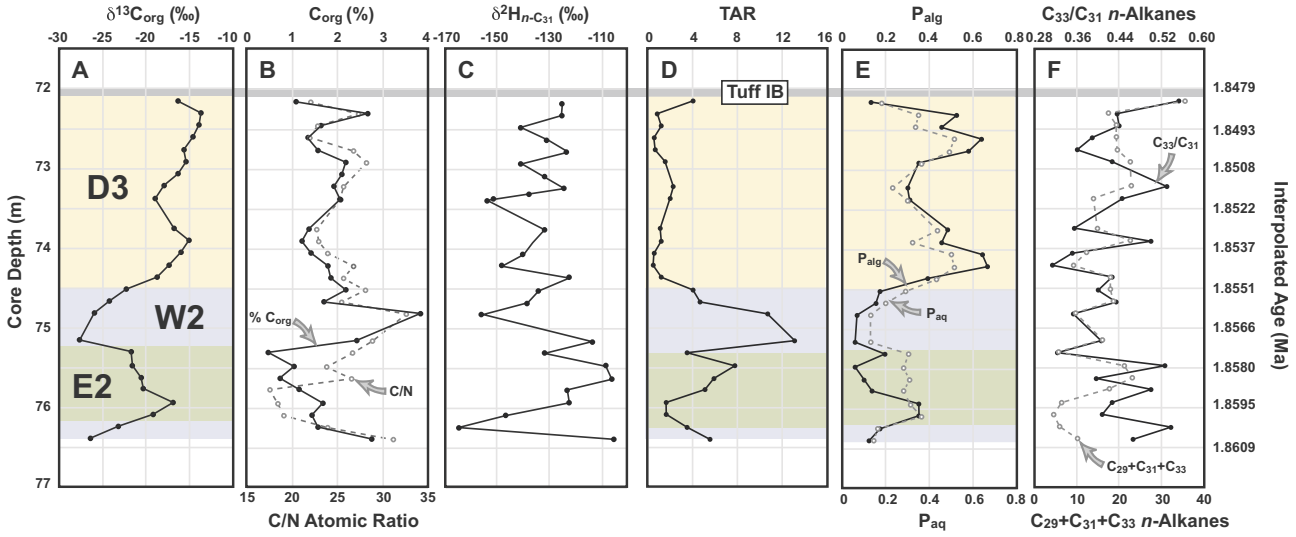

Fig. 3. Depth profiles for elemental, isotopic, and *n*-alkane data for the 72.2–76.4 m section of OGCP Core 2A with interpolated ages based on dating of the Bed I basalt and Tuff IB (Deino et al., 2020). Definitions of C/N ratios, TAR, P_{alg}, P_{aq}, and *n*-alkane ratios are described in Table 1. (A) $\delta^{13}C_{Corg}$; (B) % C_{org} (closed circles, solid line), and C/N atomic ratios (open circles, dashed line); (C) $\delta^{2}H_{nC31}$; (D) Terrigenous vs. Aquatic Ratio (TAR; Table 1); (E) P_{alg} (closed circles, solid line), and P_{aq} (open circles, dashed line); (F) C_{33}/C_{31} *n*-alkanes (closed circles, solid line) and $\Sigma C_{29} + C_{31} + C_{33}$ *n*-alkanes (open circles, dashed line). Tuff IB is shown at 72 m as a grey bar. The blue, tan, and green colors indicate the intervals designated as W2, D3 and E2, respectively. Each division between W2 and D3 is placed where statistically significant based on unpaired *t*-tests (Supplementary Table 1). (The $\delta^{13}C_{TOC}$ and C_{org} (wt%) data were previously published in Shilling et al., 2019.) (For interpretation of the references to colour in this figure legend, the reader is referred to the web version of this article.)

characterized by variations in the dominance of contributions from aquatic organisms, which may be recording fluctuations in productivity in response to nutrient supply and changes in lake salinity or alkalinity.

Fern-8-ene (Fig. 4B) can derive from either allochthonous terrestrial inputs from ferns or as an aquatic biomarker originating from anaerobic bacteria (Brassell et al., 1981; Table 1). Both potential sources are likely to increase during episodes of enhanced precipitation and run-off since they result in the transport of higher amounts of terrestrial OM into the lake and also raise or maintain elevated lake levels more conducive to generation of meromictic conditions and bottom water dysoxia. The average concentrations of fern-8-ene are consistent with these scenarios, as they are higher in W2 than in D3, albeit with major variations below 74.5 m including occurrence in only trace amounts within the 75.25 to 76.25 m interval (Fig. 4B).

Overall, the biomarker record from the 72.2–76.4 m section of OGCP Core 2A indicates that the OM within the lake sediments is dominantly derived from terrestrial sources in the wetter W2 interval (Figs. 3–5), consistent with increased precipitation and runoff during

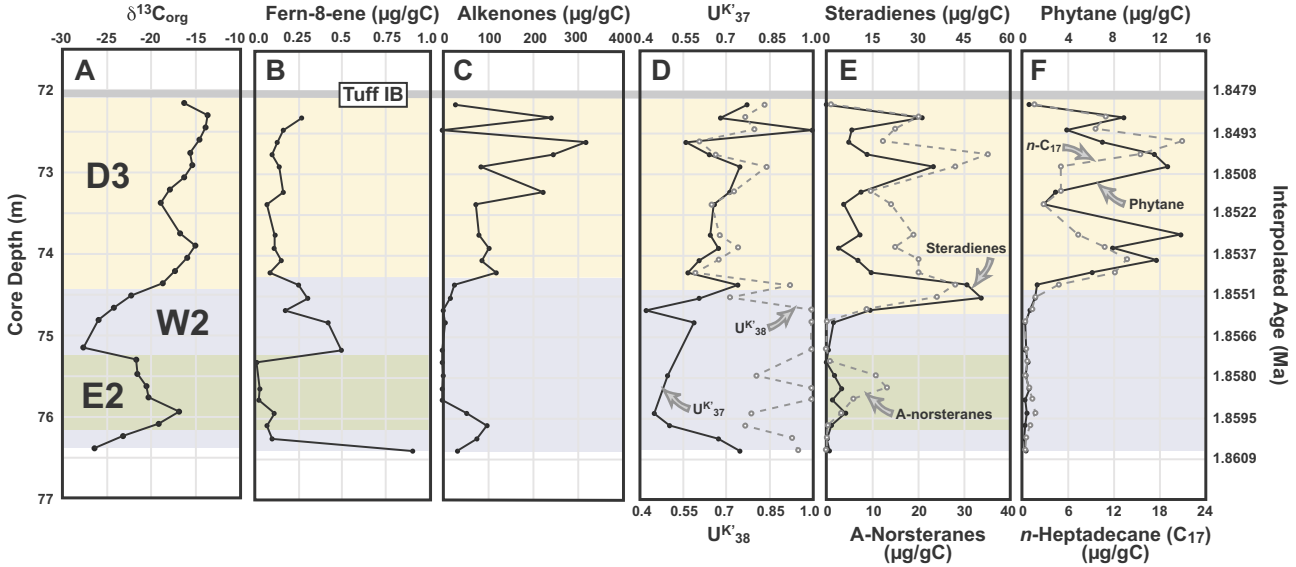

Fig. 4. Depth profiles for isotopic and molecular data for the 72.2–76.4 m section of OGCP Core 2A with interpolated ages based on dating of the Bed I basalt and Tuff IB (Deino et al., 2020). The biological sources and origins of individual biomarkers and definitions of the alkenone unsaturation indices $U^{K'}_{37}$ and $U^{K'}_{38}$ are described in Table 1. (A) $\delta^{13}C_{Corg}$; (B) Fern-8-ene; (C) Alkenones ($\Sigma C_{37:3} + C_{37:2} + C_{38:3} + C_{38:2}$; tetraunsaturated alkenones were not detected); (D) Alkenone unsaturation ratios: $U^{K'}_{37}$ (closed circles, solid lines) and $U^{K'}_{38}$ (open circles, dashed lines); (E) Steradienes ($\Sigma C_{28}\Delta^{4,22} + C_{28}\Delta^{5,22} + C_{29}\Delta^{4,22} + C_{29}\Delta^{5,22}$), and A-norsteranes ($\Sigma C_{27} + C_{28}$); (F) Phytane (closed circles, solid lines) and C_{17} *n*-alkane (open circles, dashed lines). The blue, tan, and green colors indicate the intervals designated as W2, D3 and E2, respectively. Each division between W2 and D3 is placed where statistically significant based on unpaired t-tests (Supplementary Table 1). (Data presented in A, C, D, and F were published in Shilling et al., 2019.) (For interpretation of the references to colour in this figure legend, the reader is referred to the web version of this article.)

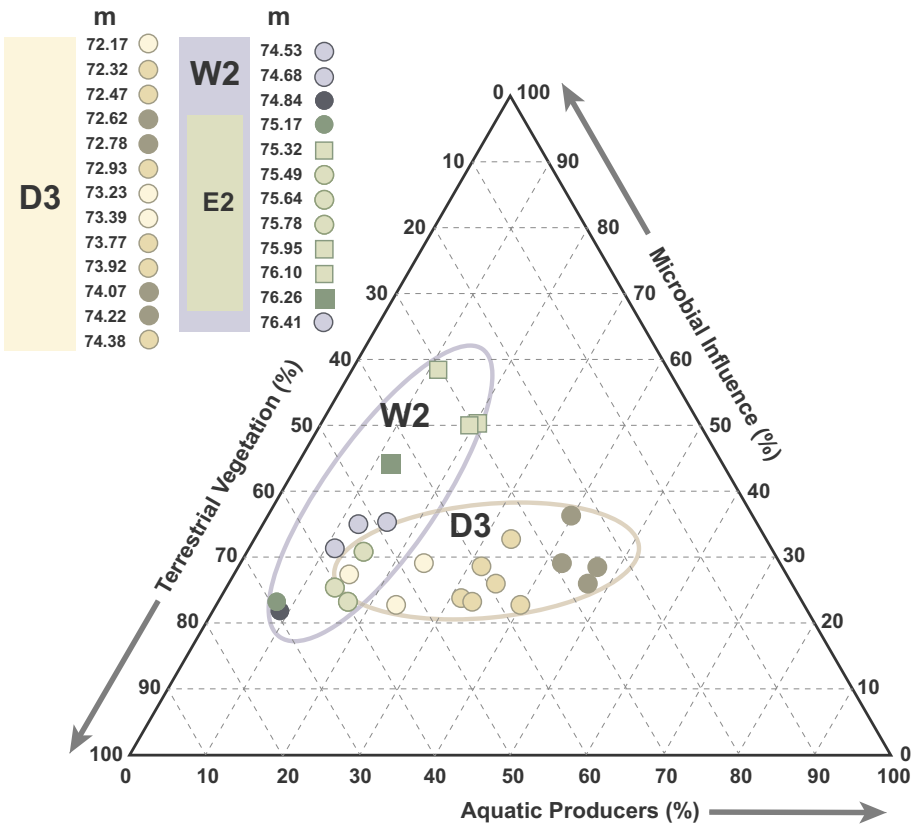

Fig. 5. Ternary plot of *n*-alkane distributions illustrating relative contributions of terrestrial vegetation, microbial influences, and aquatic producers (defined in Table 1). Each sample is colour-coded based on its *n*-alkane composition and its stratigraphic position within the W2, E2, and D3 intervals. The clusters of W2 and D3 samples show that the former vary primarily in their proportion of terrestrial vegetation, and the latter in their proportion of aquatic producers. (Modified from Shilling et al., 2019.)

this time. In contrast, the drier D3 interval is dominated by aquatic sources of OM (Figs. 3–5), as expected during an episode of decreased precipitation and runoff. This pattern of changes in the prominent sources of OM assessed by biomarkers mirrors that observed for the underlying sediments from Upper Bed I (Colcord et al., 2018, 2019).

4.2. Wetter and drier intervals within Upper Bed I

The results presented above focus on using biogeochemical data from the ~4.5 m section of core to reconstruct the depositional history of Paleolake Olduvai during the ~13 kyr immediately prior to deposition of Tuff IB and the subsequent major change in the depositional environment (Shilling et al., 2019). They reveal a pattern of wetter and drier intervals that effectively represent a continuation of the underlying section of Upper Bed I extending to the Bed I basalt (Colcord et al., 2018; Colcord et al., 2019). However, recognition of this full sequence of successive drier-wetter-drier-wetter-drier intervals (D1-W1-D2-W2-D3) facilitates consideration of the similarities and differences between individual intervals, and the associated isotope excursion events (E1 and E2) within W2, to examine evidence for longer-term trends in the data and assess the uniformity of the transitions associated with these climatic shifts.

4.2.1. Climate cycles

Temporal records of both $\delta^{13}C_{org}$ and $\delta^{2}H_{nC31}$ for the ~72–86.9 m interval of OGCP Core 2A reveal a series of alternating wetter and drier intervals (Colcord et al., 2018) that align with the Milankovitch-scale precession cycles previously identified through $\delta^{13}C_{org}$ of outcrop samples from Olduvai Gorge (Magill et al., 2013a; Fig. 6A). At noted above, the 74.5–76.4 m interval represents an extension of W2 and the section from 72 to 74.5 m constitutes an additional drier interval (D3). Statistical assessment employing box and whisker plots for C_{org}, $\delta^{13}C_{org}$ and $\delta^{2}H_{nC31}$ values for the full succession from D1 to W1 to D2 to W2 to D3 confirms that the characteristics of wetter and drier intervals are distinct (Supplementary Table 2), with the differences in $\delta^{13}C_{org}$ exhibiting the greatest contrast (Fig. 6E,F, 7B). The highest C_{org} contents of Upper Bed I occur in W1 (Figs. 6C, D, 7A), which is consistent with the presence of laminations in this interval (Colcord et al., 2018). The C_{org} contents of W2 (Figs. 6C, D, 7A) are lower, and only slightly enhanced relative to the drier intervals, suggesting that Paleolake Olduvai was perhaps shallower during deposition of W2 compared with W1, notwithstanding the possibility of a shift in the depocenter. Average $\delta^{2}H_{nC31}$ values for the drier intervals are broadly similar and also distinct from the average values for the wetter intervals (Figs. 6G, H, 7C; Supplementary Table 2). However, the range of $\delta^{2}H_{nC31}$ values for the drier and wetter intervals, except for D1, show substantive overlap and pronounced fluctuations, which may reflect short-term variations in the supply of plant wax *n*-alkanes from different source regimes within the lake catchment.

The stratigraphic profile of $\delta^{13}C_{org}$ contains two discrete positive excursions (events E1 and E2) within W2 (the earlier event was reported by Colcord et al., 2018), which are statistically distinctive (Supplementary Table 2) with $\delta^{13}C_{org}$ values akin to drier intervals (Fig. 6E, 7B). $\delta^{13}C_{org}$ values for W1 and W2 are similar when data for E1 and E2 are excluded from the latter. The individual drier intervals possess $\delta^{13}C_{org}$ values that exhibit a temporal trend (D1 to D2 to D3) toward less negative values (Figs. 6E, 7), which suggests increasing contributions from C_4 plants consistent with declining precipitation during these successive drier episodes. Each drier interval shows a progressive decrease with time in the proportion of clay material assessed from natural gamma radiation, whereas the W1 interval shows a reverse trend (Fig. 8A). However, the signal for the W2 interval, including E1 and E2, exhibits fluctuations rather than a temporal trend. The magnetic susceptibility for W2 also shows fluctuations (Fig. 8B) that coincide with the layered section of the core containing multiple sandstone intervals (cf. Fig. 2; Colcord et al., 2018), a feature that distinguishes W2 from the uniform weak signals from the rest of the ~72–87 m section of Core 2A (Fig. 8B). This stark difference between

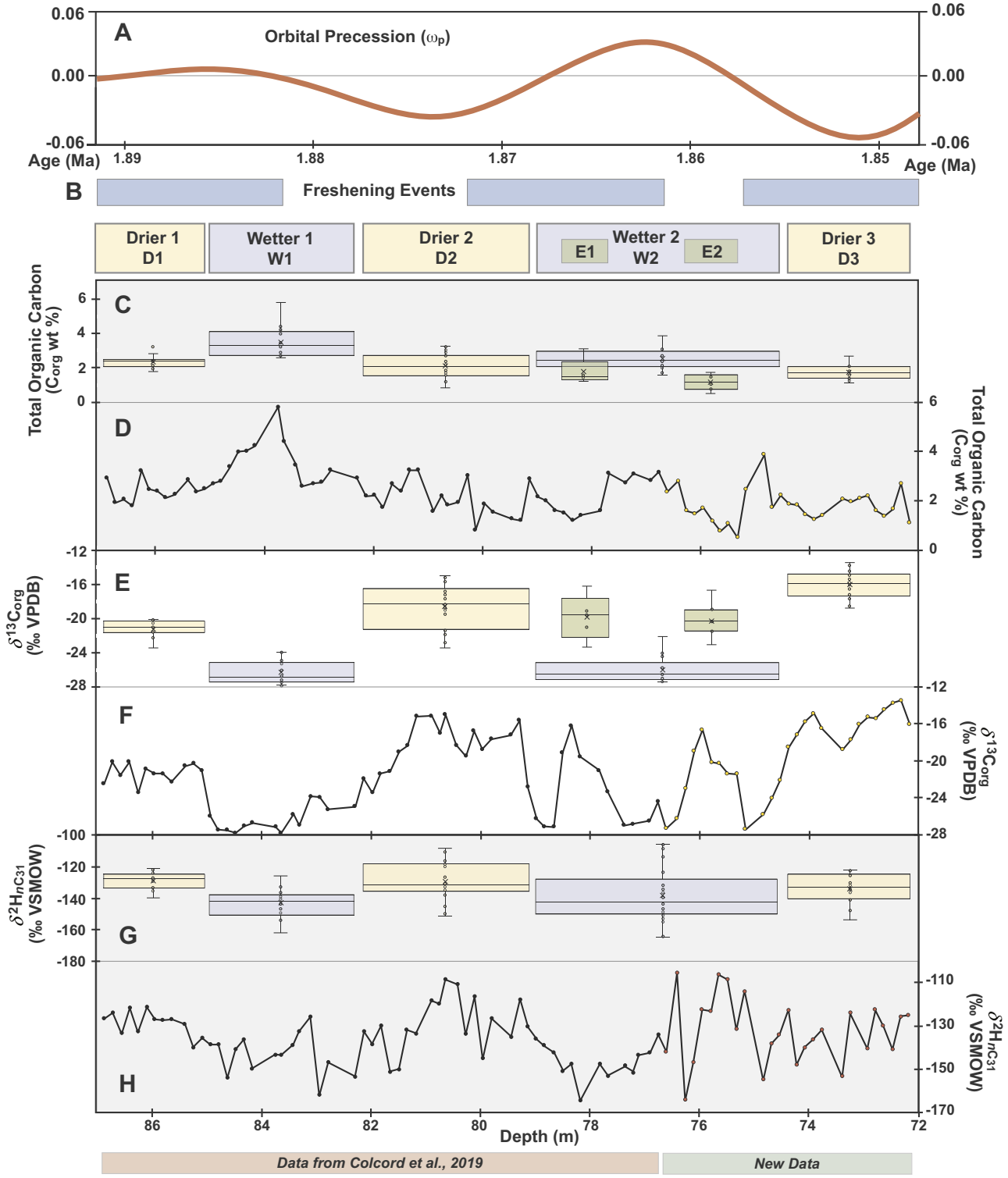

Fig. 6. Elemental and isotopic data for the Upper Bed I interval from 72 to 87 m presented as depth profiles combined with box and whisker plots for individual sections of the stratigraphic column corresponding to the three drier intervals (D1, D2, D3), two wetter intervals (W1, W2), and the two positive isotope excursion events (E1, E2) within W2. Statistical analyses of these data assessing the significance of differences between individual intervals are provided in Supplementary Table 2. (A) Temporal variations in orbital precession (Magill et al., 2013a; Deocampo et al., 2017) for interpolated ages based on dating of the Bed I basalt and Tuff IB (Deino et al. 2020); (B) Timing of freshening events based on Al_2O_3/MgO ratios for sediments from Upper Bed I at location 80 (Fig. 1; Deocampo et al., 2017); (C) Box and whisker plots for Total Organic Carbon (C_{org}; wt%). (D) Depth profile of Total Organic Carbon (C_{org}; wt%). (E) Box and whisker plots for $\delta^{13}C_{Corg}$. (F) Depth profile of $\delta^{13}C_{Corg}$. (G) Box and whisker plots of $\delta^{2}H_{nC31}$. (H) Depth profile of $\delta^{2}H_{nC31}$. Data for 76.6–86.9 m (black circles) and 72.2–76.4 m (yellow circles) intervals were previously published in Colcord et al., 2018 and Shilling et al., 2019, respectively. $\delta^{2}H_{nC31}$ data for the 72.2–76.4 m interval (red circles) are unpublished as noted by the detail below the figure. (For interpretation of the references to colour in this figure legend, the reader is referred to the web version of this article.)

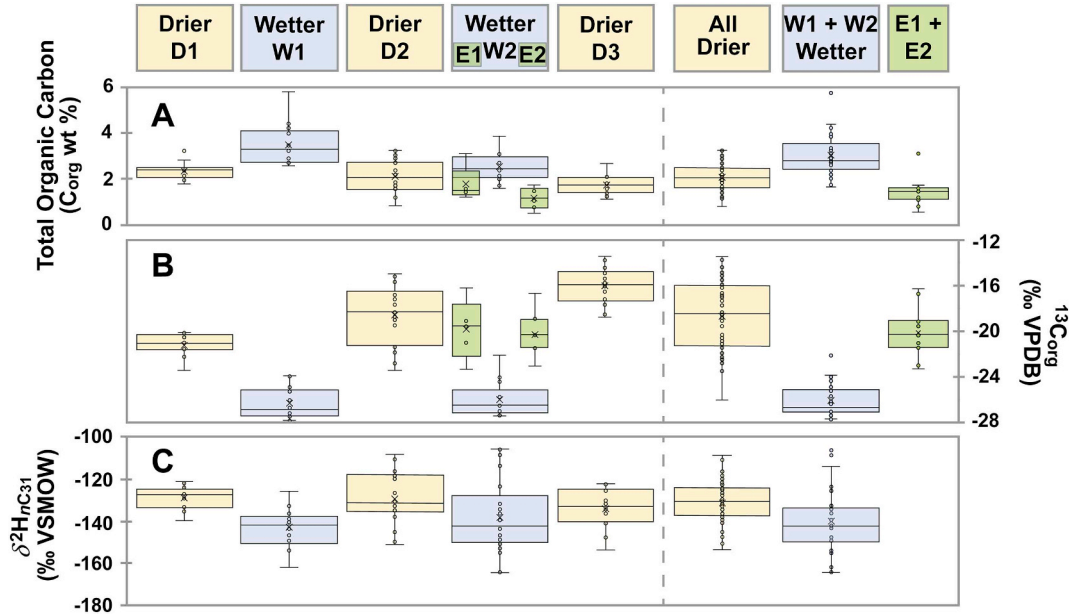

Fig. 7. Elemental (A: Total Organic Carbon; C_{org}; wt%) and isotopic (B: $\delta^{13}C_{Corg}$; C: $\delta^{2}H_{nC31}$) data for the drier intervals (D1, D2, D3), wetter intervals (W1, W2), and excursion events (E1, E2) within W2 presented as box and whisker plots, coupled with data for all three drier intervals (ΣD1 + D2 + D3), both wetter intervals (W1 + W2), and both excursion events (E1 + E2). Statistical analyses of these data assessing the significance of differences between individual intervals are provided in Supplementary Table 2.

the observed magnetic susceptibility for W2 and the remainder of the Upper Bed I section can best be explained in terms of a difference in drainage patterns or catchment, or a change in the material actively being eroded into the basin (Fig. 8B). The two clear pulses of increased natural gamma radiation within Upper Bed I occur during the E1 and E2 events likely representing episodes of higher clay input, which could reflect a decrease in precipitation that restricted transport of coarser detritus into the lake depocenter or, alternatively, flooding events (cf. Ashley et al., 2016). Direct comparison of the $\delta^{13}C_{org}$ value for each sampled interval with the magnetic susceptibility for the same horizon shows no correspondence between these parameters (Fig. 8C). Consequently, the E1 and E2 positive excursions in $\delta^{13}C_{org}$ do not appear to be directly linked to a specific change in source materials but rather likely represent episodes of lower precipitation during W2.

The W2 wetter event differs from W1 is its duration (~13 kyr versus ~7.6 kyr, based on linear age interpolation), albeit interrupted by millennial-scale isotope excursion events (E1 = ~2.57 kyr; E2 = ~2.83 kyr) representing drier intervals. Both wetter intervals overlap with the markedly longer freshening events (Fig. 6B) characterized by changes in the composition of authigenic clays (Deocampo et al., 2017). The duration of W1, but not W2, echoes evidence for an earlier sequence of wet/dry cycles (3.1–2.35 Ma) from the Chemeron Formation (Central Kenya Rift) that lacustrine conditions occur over ≤8 kyr of each precessional cycle (Deino et al., 2006).

4.2.2. Climate transitions

The shifts in $\delta^{13}C_{Corg}$ values associated with wetter to drier transitions (Fig. 9Aa, Ca) span several samples representing ~2.6 to ~4.4 kyr, whereas the drier to wetter transitions (Fig. 9Ba,Da) occur over markedly shorter timespans of <1 kyr. The disparity in the timing of the transitions could result from differences in the rate of change in precipitation during these climate transitions whereby increases in rainfall occur faster than declines. An increase in the flux of OM from soils resulting from higher runoff associated with the drier to wetter transition could either induce more effective purging of the accumulated reservoir of less negative $\delta^{13}C_{Corg}$ or prolong inputs of less negative $\delta^{13}C_{Corg}$ from such OM reservoirs unless the latter possibility is negated by preferential decomposition of C_4 plant material in soil (Wynn and Bird, 2007). Alternatively, and perhaps more likely, is the possibility that an increase in precipitation induces a rapid response in terrestrial vegetation leading to prompt changes in $\delta^{13}C_{org}$ values, whereas contributions from C_3 plants may persist while precipitation declines leading to a slower modulation of their signal.

The observed changes in the concentrations of sedimentary biomarkers to the different transitions shows some consistency, perhaps most evident in the measures of salinity (MTTCs) and terrestrial vegetation (TAR) which directly parallel with the changes in $\delta^{13}C_{Corg}$ values (Fig. 9). The increase in fern-8-ene concentrations accompanying drier to wetter transitions (Fig. 9Bc, Dc) appears delayed, which could reflect the time necessary for the development of dysoxic conditions within the lake as it deepens. There are also differences in the timing of the response of aquatic biomarkers within individual transitions. For example, the peak in steradienes and A-norsteranes occurs prior to the increase in alkenones for the W2 to D3 transition (Fig. 9Aa, d). The alkenone distributions are indicative of a Type II haptophyte source, which occur in saline and alkaline environments (Coolen et al., 2004; Theroux et al., 2010; Toney et al., 2012; D'Andrea et al., 2016; Longo et al., 2016), suggesting that substantive haptophyte productivity may have been delayed until the increase in lake salinity resulting from decreased precipitation and runoff reached a critical threshold more conducive for these algae. However, a pronounced increase in the abundance of steradienes and A-norsteranes only occur at the culmination of the W1 to D2 transition based on $\delta^{13}C_{Corg}$ values (Fig. 9Ca, d). Changes in the abundance of n-C_{17}, n-C_{23} and P_{alg} all show a progressive decrease associated with the D1 to W1 transition (Fig. 9De) and a progressive increase during the W2 to D2 transition (Fig. 9Ae), reflecting the fact that conditions are more favorable for cyanobacteria, algae, and macrophyte productivity under drier conditions. The temporal changes in these aquatic biomarkers across the other transitions is more complex (Fig. 9Be, Ce), which may potentially reflect variability in the source(s) of sediment. In particular, the D2 to W2 transition is comprised of a layered sequence of sandstones, sandy claystones, and claystones (Fig. 9; Colcord et al., 2018), which likely influences the proportion of allochthonous OM, and therefore the abundance of aquatic biomarkers, within the individual layers.

The evidence for changes in precipitation provided by $\delta^{2}H_{nC31}$

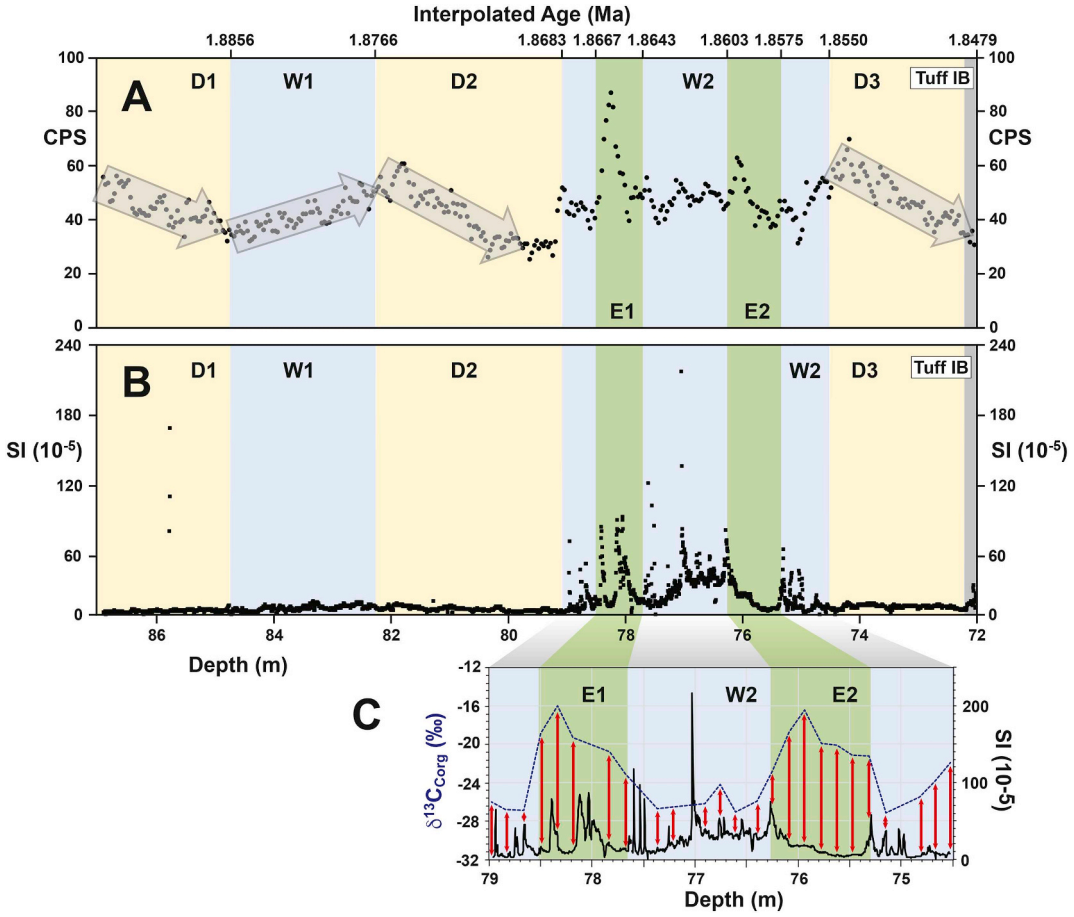

Fig. 8. Selected physical properties for the Upper Bed I core section (72–87 m) with the drier (tan) and wetter (blue) intervals and excursion events (green) shown in addition to the interpolated ages for each transition based on dating of the Bed I basalt and Tuff IB (Deino et al., 2020). (A) Natural gamma radiation measured by whole core scanning at 3.8 cm resolution. Higher values indicate sediments with higher clay content. The progressive decrease in natural gamma radiation during all three drier intervals and the increase during W1 are indicated by dark grey arrows. (B) Magnetic susceptibility measured on a split core at 0.5 cm resolution. Higher values during W2 suggest increased erosion/run off during this interval and the possibility of different drainage patterns compared with W1. (C) Illustration of the sampling resolution for $\delta^{13}C_{org}$ (red arrows represent each 3 cm sample) in comparison with magnetic susceptibility for the W2 interval, including the excursion events. The physical properties data was provided by LacCore (National Lacustrine Core Facility), Department of Earth Sciences, University of Minnesota – Twin Cities. (For interpretation of the references to colour in this figure legend, the reader is referred to the web version of this article.)

values show that the changes from a drier to a wetter climate and vice versa do not appear as smooth transitions at the temporal resolution (i.e. ~90 yr integrated signals at ~460 yr intervals) afforded by the sampling. The inter-sample fluctuations evident in lithological differences may again reflect variations in the source(s) of OM from proximal and distal parts of the lake catchment, augmented by the supply of plant waxes eroded from soil reservoirs and the potential for contributions via eolian deposition.

5. Discussion

5.1. Pleistocene paleoclimate and paleoenvironment of Paleolake Olduvai

5.1.1. Environmental setting preceding deposition of Tuff IB

The nature of Paleolake Olduvai recorded at OGCP Site 2A appears to have changed radically after deposition of Tuff IB becoming shallower, and perhaps ephemeral (Shilling et al., 2019), in stark contrast to its earlier characteristics (Colcord et al., 2018, 2019). The evidence for desiccation between Tuffs IB and IF (Shilling et al., 2019) contrasts with the assessment that Paleolake Olduvai continued to experience wet/dry cycles during this interval (Ashley, 2007). It is therefore pertinent to consider whether there are aspects of the prior history of the environment of Paleolake Olduvai that serve as prescient indicators of its subsequent fate. Evaluation of the isotopic and molecular signatures (Figs. 3, 4) for the 74.5 to 76.4 m section of OGCP Core 2A show that it represents a continuation of a wetter phase of deposition designated as W2 (Colcord et al., 2018, 2019). The overlying 74.5 to 72.2 m section resembles a drier interval, designated as D3 that yielded $\delta^{13}C_{Corg}$ values similar to the earlier D1 and D2 intervals (Colcord et al., 2018; Figs. 6, 7). Exceptions to this pattern are the C_{org} contents and C/N ratios, which differ little in terms of average values between the two intervals (Fig. 3B). Both geochemical measures exhibit greater variability in W2, which is likely attributable, in part, to the lithological differences associated with the layering that occurs within this interval. The $\delta^{13}C_{Corg}$ values for the W2 wetter interval indicate an environment dominated by C_3 plants (cf. Magill et al., 2013a, 2013b), although there is also a pronounced carbon isotope excursion event, where $\delta^{13}C_{Corg}$ reaches values almost comparable to those characteristic of the drier intervals (Figs. 4, 5A, 6A). For the drier D3 interval $\delta^{13}C_{Corg}$ values suggest an environment dominated by C_4 plants, likely to include drought-resistant plants such as grasses, perhaps complemented by sedges (Magill et al., 2013b). Fluctuations in the depth profile of the C_{33}/C_{31} *n*-alkane ratio (Fig. 3F; Bush and McInerney, 2013) confirm that the contributions from grasses are variable at the sampling resolution employed, perhaps reflecting changes in OM sources associated with lithological differences. The W2 to D3 transition therefore contrasts markedly with the

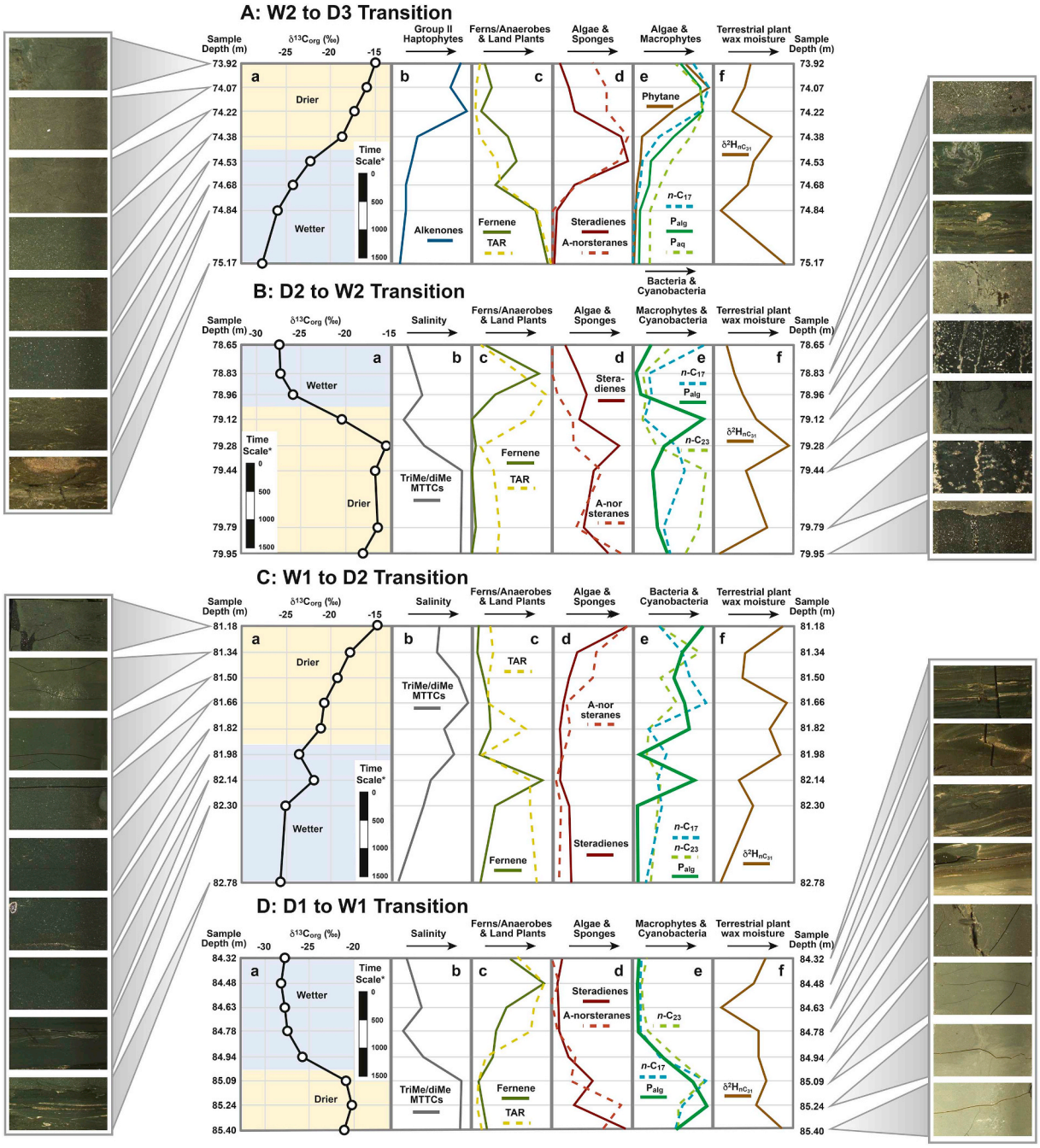

Fig. 9. Photographs of individual samples spanning the four major climate transitions – (A) W2 to D3, (B) D2 to W2, (C) W1 to D2, and (D) D1 to W1 – in the 72–87 m section of OGCP Core 2A and depth profiles of their biogeochemical data. Data for B, C, and D are taken from Colcord et al., 2018, 2019. Each transition includes depth profiles for: (a) $\delta^{13}C_{org}$ (black line), noting the depth of the transition and the time scale derived from linear age interpolation based on dating of the Bed I basalt and Tuff IB (Deino et al., 2020); (b) relative salinity (grey line) based on the ratio of trimethyl to dimethyl MTTCs (Table 1), or abundance of alkenones (blue line) representing Group II haptophytes associated with saline/alkaline lakes; (c) fern-8-ene (green line) and TAR (dashed gold line; Table 1) reflecting ferns/anaerobes and land plants, respectively; (d) steradienes (red line) and A-norsteranes (dashed red line) derived from algae and sponges, respectively; (e) algae and macrophytes based on P_{alg} (solid green line) and P_{aq} ratios (dashed green line; Table 1), cyanobacteria (n-C_{17}; dashed blue line), and bacteria (phytane; brown line); (f) δ^2C_{nC31} (brown line) reflecting changes in precipitation recorded in plant waxes. (For interpretation of the references to colour in this figure legend, the reader is referred to the web version of this article.)

more uniform, systematic variations in the C_{33}/C_{31} n-alkane ratio observed for the earlier wetter/drier cycles (D1 to W2 to D2; Colcord et al., 2019).

The biomarker composition of sediment samples from the W2 interval reveal lower abundances of components derived from aquatic producers and higher contributions from terrestrial vegetation, as indicated by n-alkane distributions (Figs. 3, 4, 5). The biomarker composition of the D3 section, in stark contrast to W2, includes higher contributions from aquatic sources complemented by lower concentrations of components derived from terrestrial vegetation (Fig. 4), comparable to other drier intervals. Differences in the sources of OM between the W2 and D3 intervals are perhaps best expressed by representation of their n-alkane distributions in a ternary diagram (Fig. 5). The major variable in W2 is the relative proportions of

terrestrial versus microbial components whereas for D3 is it the prominence of aquatic sources. Thus, for the W2 interval it appears that inputs of OM vary between: (i) a predominance of contributions from plant waxes resulting from increased precipitation and runoff, and (ii) increased microbial influence likely reflecting, at least in part, more degraded OM perhaps derived from soil accumulations formed during episodes of lessened rainfall. For the D3 interval the major controlling variable may be the supply of nutrients fueling phytoplankton productivity.

The excursion event (E2) in $\delta^{13}C_{Corg}$ recognized toward the end of the W2 interval (Figs. 3, 4) resembles a similar feature (E1) in the earlier section of the W2 interval (Colcord et al., 2018). Both excursion events are associated with lower values for TAR ratios and fern-8-ene concentrations, plus higher P_{alg} ratios, suggesting that contributions from terrestrial vegetation declined during these events. Thus, E1 and E2 appear to represent short-term drier episodes within a wetter interval, as suggested by their C_{org} and $\delta^{13}C_{Corg}$ values (Fig. 6), which indicate that they may reflect: (i) a millennial-scale decrease in precipitation, or (ii) changes in drainage patterns within the catchment area of Paleolake Olduvai. The former interpretation would imply variations in precipitation during W2 making it significantly different from the preceding wetter interval (W1). The latter possibility is consistent with the evidence for variations in the sources of sediments during W2 provided by magnetic susceptibility measurements (Fig. 8). Progressive development of the Olmoti fan may have been a contributing factor, likely modifying the configuration of the Olduvai basin and thereby changing its hydrologic patterns, including groundwater, which could have affected water supply to Paleolake Olduvai and its catchment area. The duration of the E1 and E2 events (~2.6 and ~ 4.4 kyr) is broadly comparable to Dansgaard-Oeschger oscillations (Dansgaard et al., 1989), which are well expressed in sediment records from the North Atlantic (Raymo et al., 1998) where they have been linked to ice sheet dynamics (Weirauch et al., 2008). The occurrence of climate cycles with a 1450 yr periodicity, first recognized in ice cores (Dansgaard et al., 1969), appears to be associated with oscillations in atmospheric circulation related to monsoonal climate (Mayewski et al., 1997). The existence of the 1450 yr periodicities in the flux of terrigenous material for a 24 kyr sediment sequence from the Arabian Sea has been coupled to summer dust discharge from the Arabian peninsula (Sirocko et al., 1996). Hence, the E1 and E2 events may represent a teleconnection to monsoonal circulation in the Arabian Sea, although their occurrence at ~1.855 Ma long predates other records of such periodicities in the region. A further critical feature of the events is the timing of the advent of E1 and the termination of E2. Both of these transitions are defined by successive samples indicating that they occurred in < ~460 yr, which is faster than the changes in precipitation associated with wet/dry cycles.

The overall, long-term trend exhibited by the lacustrine deposits that comprise the sedimentary Upper Bed I sequence between the Bed I Basalt (~90 m) and Tuff IB (~72 m) suggests increasing aridity in the sequence of precession-driven wet-dry cycles. Specifically, the average values of $\delta^{13}C_{Corg}$ for the succession of drier intervals (D1, D2, D3) show a progressive increase (Figs. 6, 7; Supplementary Table 2), which can be attributed to an environment becoming more favorable for drought-resistant C_4 plants, such as grasses, rather than a woodland habitat dominated by C_3 plants (cf. Magill et al., 2013a, 2013b). The occurrence of two, millennial-scale drier events (E1 and E2) during W2 suggests that this wetter interval was more prone to perturbation than its predecessor, W1, whether resulting from local or regional controls on precipitation and runoff. In addition, laminated sediments were deposited during W1 (Colcord et al., 2018) but are absent in W2 indicating that Paleolake Olduvai was likely significantly deeper during the former wetter interval. Thus, the dramatic change in the depositional environment of Paleolake Olduvai that occurred between Tuffs IB and IF and lead to its frequent desiccation after the D3 drier interval (Shilling et al., 2019) appears to represent a continuation of the trend of increasing aridity within the drier intervals of Upper Bed I. However, increased degradation of the biomarker record after deposition of Tuff IF obfuscates the climate signals and the ability to distinguish the triggers for the overall drying trend, especially how it relates to changes in drainage patterns within the Olduvai Basin. Consequently, the depositional record at OGCP Site 2A does not reveal wet/dry lake cycles between Tuffs IB and IF akin to those reported in the sediment sequence from the western lake margin (Ashley, 2007).

5.1.2. Temporal resolution of biogeochemical proxies from aquatic and terrestrial sources

A key objective in biogeochemical analyses of sediments from OGCP Core 2A is to determine paleoclimate records at higher resolution than attainable from studies of outcrops (Magill et al., 2013a, 2013b). The chosen sampling protocols achieve that aim, yielding ~90 yr integrated signals at ~460 yr intervals throughout Upper Bed I (Colcord et al., 2018, 2019; Shilling et al., 2019). However, comparison of the depth profiles for biogeochemical and physical properties data (Fig. 8C) illustrates the differences in temporal resolution whereby measurements of magnetic susceptibility and natural gamma radiation taken every 0.5 cm and 3.8 cm, respectively, identify lithological distinctions not accessible via collection of 3 cm samples at 16 cm intervals. Hence, the coarser resolution of the biogeochemical records likely precludes recognition of some of the sedimentary variability shown by the physical properties data. The loss of climate signals through sedimentary aliasing is evident and prevalent in the $\delta^{13}C_{Corg}$ records of OGCP Core 3A (Ferland et al., 2020), whereas the 3 cm samples for biomarker analyses (Fig. 8) appear unable to cannot capture differences between horizons within the thinly layered section of the core from ~74.5 to 75.5 m depth of OGCP Core 2A where individual layer thicknesses are sub-cm scale. Sediments in other parts of Upper Bed I (cf. Fig. 2) appear homogenous at 3 cm resolution, which suggests that their ~90 yr averaged signals are indeed representative of OM sources and depositional conditions over this time window.

Yet, comparisons of the depth profiles for terrestrial and aquatic biomarkers prompts consideration of potential differences in their temporal and spatial resolution. For autochthonous components, each 3 cm sample provides an integrated signal of lake productivity over ~90 yr based on the age-interpolated sediment accumulation rate of ~0.35 $mmyr^{-1}$. Allochthonous contributions of OM assessed using plant wax *n*-alkanes, $\delta^{13}C_{Corg}$, and $\delta^{2}H_{nC31}$ similarly represent a ~ 90 yr record of deposition, although these proxies likely comprise a longer-term integrated signal of terrestrial vegetation because they reflect: (i) non-uniform delivery from different areas within the lake catchment dependent on local precipitation patterns and transport pathways (Pu et al., 2017), (ii) the different residence times of lipids and OM within the terrestrial ecosystem (Douglas et al., 2014; Pu et al., 2018), and (iii) contributions from erosion of OM accumulated in soils over variable timespans (Seki et al., 2010; Wu et al., 2019). Thus, the ability to decipher short-term variations in terrestrial vegetation, such as shifts in C_3 versus C_4 plants and precipitation, is constrained by both sampling resolution and the processes controlling how terrestrial signatures are conveyed, integrated, and preserved within the sedimentary record. Investigation of proxies for plant waxes within individual horizons of the layered sequence at ~75 m would help determine whether discrete signals associated with short-term depositional events can be discerned within Upper Bed I. In addition, it is appropriate to evaluate how the sedimentary record of terrestrial vegetation varies with changes in precipitation associated with the wet/dry cycles and assess the rate of response of biogeochemical proxies to such transitions in climate.

5.1.3. Climate transitions

The stratigraphic profiles of elemental, isotopic and molecular compositions during the transitions from drier to wetter conditions, and vice versa, provide evidence of biogeochemical responses to these changes in the lake environment, especially the signals manifest in

terrestrial and aquatic biomarkers. Divisions between wetter and drier intervals are primarily based on stratigraphic variations in $\delta^{13}C_{Corg}$ values (Figs. 3, 6, 7) with transitions from drier to wetter conditions occurring faster (~900 yr) than the reverse trend (~2.6–4.4 kyr; Fig. 9) suggesting that isotopic signals from terrestrial vegetation exhibit a more rapid response to increased precipitation than to its decline. These timings broadly correspond with conceptual models that portray a progressive rise (~1 kyr) and more gradual decline (~2.5 kyr) in East African lake levels during wet/dry cycles, reflecting variations in precipitation resulting from changes in precession (Trauth et al., 2010). However, the transitions associated with development of E1 and termination of E2 are even shorter (< ~460 yr) suggesting that the terrestrial ecosystem has the capacity to respond on these timescales, notwithstanding the possibility that all transitions may reflect shifts in the principal source(s) of sedimentary OM rather than a comprehensive change in regional vegetation.

The ability to determine and distinguish the timescales of these transitions reflects the sampling resolution afforded by OGCP Core 2A but the absence of comparable data documenting the timespan of alternating millennial-scale shifts in $\delta^{13}C_{Corg}$ values for other lake sediments from East Africa or elsewhere precludes the possibility of assessing whether the differences in the timing of climate transitions at Olduvai are the norm for the region and representative of similar shifts from wet to dry conditions and vice versa in the geological past.

As expected, most of the trends in biogeochemical proxies that are observed for wetter to drier transitions tend to be reversed for drier to wetter transitions, although the timing, rate, and magnitude of the change in the responses often differs (Fig. 9). The proxy that shows the closest parallel to the changes in $\delta^{13}C_{org}$ values is the ratio for MTTCs (methyltrimethyltridecylchromans; Sinninghe Damsté et al., 1987), which serves as an indicator for salinity. For the W2 to D3 transition the increase in alkenone abundance also likely reflects a salinity trend as these compounds are synthesized by haptophytes within the Group II phenotype that favor saline/alkaline conditions (Coolen et al., 2004; Theroux et al., 2010; Toney et al., 2012; D'Andrea et al., 2016; Longo et al., 2016). Thus, the salinity of Paleolake Olduvai appears to match the shift in $\delta^{13}C_{org}$ values, which reinforces the interpretation that terrestrial vegetation in the region is controlled by precipitation changes associated with wet/dry climate cycles that govern water supply to the lake.

None of the biomarker indices closely matches the systematic trends in $\delta^{13}C_{org}$ values for every transition; the proxies all show fluctuations in their relative abundance across the transitions that indicate short-term variations in their depositional flux. Indeed, the progressive changes in $\delta^{13}C_{org}$ associated with the transitions derive from the fact that it represents an integrated signal of the source(s) of OM, in contrast to biomarkers that represent signatures of specific contributions prone to short-term temporal variations. The biogeochemical proxies reflecting terrestrial vegetation (e.g., TAR index; Fig. 9) tend to vary inversely with $\delta^{13}C_{org}$ values, albeit with varying degrees of conformity for the different transitions. Among aquatic biomarkers steradienes and A-norsteranes derived from algae and sponges, respectively, became more prominent contributors of OM under drier conditions, but with some inconsistency in the timing of changes in their abundance as they may either precede or follow the shift in $\delta^{13}C_{org}$ values (Fig. 9d). Similarly, the overall proportions of algal/cyanobacteria and aquatic macrophytes, as measured by P_{alg} and n-C_{17} and by P_{aq} and n-C_{23}, respectively (Ficken et al., 2000; Magill et al., 2013a), also vary in the nature of their response to the transitions (Fig. 9e). In effect, smooth and progressive changes in $\delta^{13}C_{org}$ values associated with the climate transitions from wetter to drier conditions and vice versa are not always matched by similarly uniform trends in aquatic biomarkers whose abundance is controlled by environmental factors other than precipitation. The specific lake characteristics that influence the prevalence of biota producing individual components likely include salinity (alkenones), nutrient supply supporting algal productivity (steradienes, n-C_{17}, P_{alg}) and turbidity limiting it, freshwater inflow and ponds (A-norsteranes), and the prevalence of shallow water habitats suitable for macrophytes (P_{aq}, n-C_{23}). Many of these aspects of Paleolake Olduvai would have been directly affected by precipitation and runoff, especially the impact of these environmental changes on the size and extent of the lake, but would also be subject to changes in lake dynamics and geometry associated with sediment deposition and tectonic events. Moreover, unlike terrestrial vegetation, phytoplankton and aquatic plants can respond rapidly to short-term environmental perturbations and generate biogeochemical signals that record such episodes in lake sediments (Hanisch et al., 2003, 2009), which is emblematic of the inherent differences between terrigenous and aquatic proxies.

5.2. Significance of climatic variability for hominin evolution

A persistent theme in efforts to connect hominin evolution with climate drivers is concern for the timing and magnitude of environmental changes and how they would have affected the resources available to different hominin populations (deMenocal, 1995, 2011; Shultz et al., 2012; Potts, 2013; Antón et al., 2014; Maslin et al., 2014, 2015; Potts and Faith, 2015). Confirmation of wetter and drier intervals within the stratigraphic sequence deposited in Paleolake Olduvai between the Bed I Basalt and Tuff IB (Figs. 6, 7) related to precession-scale variations in precipitation (Deino et al., 2006; Ashley, 2007; Maslin et al., 2014) echoes prior interpretations that the landscape varied from a dominance of woodlands to grasslands (Magill et al., 2013a, 2013b). However, $\delta^{13}C_{org}$ records from OGCP Core 2A now help to constrain the timescales of the shifts in terrestrial vegetation associated with transitions from drier to wetter and wetter to drier climate, revealing that the steadfast changes for the former occurred over ~900 yr whereas those for the latter took significantly longer, > 2.6 kyr. Yet, the timing of the isotope excursion events, E1 and E2, show that more rapid transitions (< ~460 yr) also appear in the OGCP core 2A record in shifts toward drier and then wetter climate. The occurrence of two millennial-scale (~2.6 and ~4.4 kyr) excursion events in W2 (Figs. 6, 7), likely representing a decrease in precipitation, confirms that there are significant environmental changes independent of precession-scale wet/dry cycles that likely affected the resources available to hominins in the Olduvai region.

Shifts in $\delta^{13}C_{org}$ values for sediments from Paleolake Olduvai reflect changes in contributions from terrestrial vegetation, especially variations in the proportions of C_3 versus C_4 plants. An increase in C_3 plants following development of wetter conditions would be reflected by increased woodland vegetation (Magill et al., 2013a, 2013b) and therefore more shade for hominin activities (Magill et al., 2016). By contrast, a greater proportion of C_4 plants as conditions became drier could correspond to more grasses but also enhanced populations of macrophytes, including sedges that may serve as an important food source for *Paranthropus boisei* (Cerling et al., 2011). The evidence from biogeochemical proxies indicative of macrophytes, P_{aq} and n-C_{23}, supports this possibility as they both increase during drier intervals. In addition, the higher inputs from A-norsteranes implies a persistence of freshwater in areas of the lake margins thereby providing a critical resource for hominins, even as the lake become more saline (Fig. 9).

The timescale (~460 yr to 4.4 kyr) of environmental changes associated with both the transition from wetter to drier climate and vice versa and the millennial-scale drier intervals are all gradual in terms of individual hominin lifespans but result in marked differences in the vegetated landscape and fluctuations in lake resources over multiple hominin generations. Thus, abrupt episodes of volcanism manifest in the deposition of tuffs probably have greater potential for short-term environmental perturbation than the timing of shifts in climate, especially precipitation, based on evidence from biogeochemical proxies. However, the evidence for a progressive trend toward increasing aridity from D1 to D3 (Figs. 6, 7), followed by desiccation after deposition of

Tuff IB (Shilling et al., 2019), represents a longer-term, stepwise change in Paleolake Olduvai from a deeper lake setting to a shallow, ephemeral lake that may have profoundly affected the nature and availability of food and shelter for hominins, and access to key resources. The combination of repetitive environmental and climatic changes may therefore have served to help support and sustain diverse hominin populations adapted to use of distinct resources.

6. Conclusions

Investigation of elemental, isotopic, and molecular compositions of sedimentary OM from the lacustrine section of OGCP Core 2A deposited immediately prior to Tuff IB yields high-resolution records of environmental and climate records at Olduvai Gorge at ~1.85 Ma. A combination of biogeochemical proxies (C_{org}, $\delta^{13}C_{TOC}$, $\delta^{2}H_{nC31}$, and terrestrial & aquatic biomarkers; Figs. 3, 4; Table 1), complemented by sedimentological descriptions and physical properties data (Figs. 2, 8), expand the sequence of precession-scale wet/dry climate cycles established for Upper Bed I. They extend the previously identified second wetter interval (W2) and reveal its transition into a third drier interval (designated D3) based on the same range of proxies (i.e., $\delta^{13}C_{org}$, terrestrial vs. aquatic biomarkers) used to characterize the earlier wetter and drier intervals (Figs. 6, 7). In addition, a second drier event (E2) was identified within W2 based on stratigraphic variations in $\delta^{13}C_{org}$ and C_{org} (Figs. 3, 4, 6, 7), suggesting that the lake environment was more prone to drying episodes during this time. The two millennial-scale events (E1 and E2, lasting ~2.6 and ~ 4.4 kyr, respectively, based on interpolated ages) within W2 illustrate the sensitivity of the Paleolake Olduvai environment to a combination of changes in precipitation, variations in water supply attributable to groundwater and drainage dynamics, and modifications in lake bathymetry from progressive development of Olmoti fan deposits. Longer-term (~9 kyr) shallowing of the lake is supported by the difference between the sedimentary records of the W1 and W2 intervals. The W1 interval is characterized by laminated sediments and high C_{org} contents suggesting that Paleolake Olduvai was meromictic, whereas these diagnostic features are absent in W2, which shows greater susceptibility to drying based on the presence of the excursion events. Further evidence for gradual environmental changes is afforded by differences among the three successive drier events (D1, D2, and D3), which record a trend toward higher $\delta^{13}C_{org}$ values corresponding to a sequential increase in the proportion of C_4 plants during these intervals, consistent with declining precipitation. These events perhaps serve as a prelude to the post-Tuff IB desiccation of Paleolake Olduvai.

Interpolation of the sediment accumulation rate for the Upper Bed I sequence based on ages for the Bed I basalt and Tuff IB (Deino et al., 2012) constrains the timing and rate of climate shifts associated with the wet/dry cycles, revealing that the response of terrestrial vegetation to transitions from drier to wetter conditions, as recorded by $\delta^{13}C_{Corg}$, is faster (~900 yr versus > 2.6 kyr) than from wetter to drier conditions. For the drier events shown by excursions in $\delta^{13}C_{Corg}$ the onset of E1 and the termination of E2 are both expressed as shifts in values between successive 3 cm samples (each representing an integrated ~90 yr signal) collected with 16 cm spacing, and thereby corresponding to a climate-driven change in sediment inputs in <~460 yr. The temporal profiles of several aquatic biomarkers (e.g. alkenones, steradienes, n-C_{17}) also exhibit marked differences in their concentrations between successive samples (Fig. 4) reflecting subtle, nuanced responses of phytoplankton communities to changes in the lake environment on centennial timescales. Abrupt variations in aquatic biomarkers appear more prevalent than those observed for proxies of terrestrial vegetation, which reinforces the perspective that the lake's aquatic ecosystem responds more dynamically to changes in climate than the terrestrial ecosystem. Thus, the availability of aquatic resources for hominins, including freshwater and macrophytes, may have been subject to greater and faster fluctuations than variations in terrestrial vegetation, including the relative proportions of woodland and grassland settings. Further investigation of the rates of climatic change is undoubtedly merited and could be achieved through sampling of OGCP Core 2A at higher temporal resolution. Greater stratigraphic resolution of biogeochemical proxies would potentially clarify the pace of landscape transitions and the temporal variability of aquatic organisms within Paleolake Olduvai and its margins thereby making it possible to access potential influences on hominin evolution through understanding environmental changes at timescales comparable to hominin lifespans.

Supplementary data to this article can be found online at https://doi.org/10.1016/j.palaeo.2020.109824.

Declaration of Competing Interest

The authors declare that they have no known competing financial interests or personal relationships that could have appeared to influence the work reported in this paper.

Acknowledgements

We would like to acknowledge and thank the Stone Age Institute for organizing and funding the Olduvai Gorge Coring Project (OGCP) with grants from the Kamen Foundation, the Gordon and Ann Getty Foundation, the John Templeton Foundation, the Fred Maytag Foundation, Kay and Frank Woods, and NSF (BCS1623873). Additionally, we are grateful to the Tanzanian Commission for Science and Technology, Tanzanian Department of Antiquities, Ministry of Natural Resources & Tourism, and the Ngorongoro Conservation Area Authority (NCAA) for enabling the collection of samples and continuing support of OGCP research. Support for biomarker preparation included funds provided by the Department of Earth and Atmospheric Sciences (Indiana University). NSF grant CHE1726633 enabled purchase of the GC-QTOF-MS (Mass Spectrometry Facilities at Indiana University) utilized in this study for all biomarker analyses. We would like to thank Dr. Al Deino (UC Berkeley) and coauthors for sharing new chronological data for OGCP Core 2A prior to publication and Dr. Arndt Schimmelmann (Indiana University) for providing both an n-alkane standard mix, and the squalane standard. In addition, we would like to thank LacCore for their assistance with core handling and sample collection, as well as providing the core scan data. The manuscript also benefited from the comments of anonymous reviewers that prompted extensive revisions.

References

Ageta, H., Arai, Y., 1983. Fern constituents: pentacyclic triterpenoids isolated from *Polypodium niponicum* and *P. formosanum*. Phytochem. 22, 1801–1808. https://doi.org/10.1016/S0031-9422(00)80275-7.

Ageta, H., Shiojima, K., Arai, Y., 1968. Fern constituents: neohopene, hopene-II, neohopadiene, and fernadiene isolated from *Adiantum* species. Chem. Commun. (London) 1105–1107. https://doi.org/10.1039/C19680001105.

Agusti, J., Lordkipanidze, D., 2011. How "African" was the early human dispersal out of Africa? Quat. Sci. Rev. 30, 1338–1342. https://doi.org/10.1016/j.quascirev.2010.04.012.

Albert, R.M., Bamford, M.K., 2012. Vegetation during UMBI and deposition of Tuff 1F at Olduvai Gorge, Tanzania (ca. 1.8 Ma) based on phytoliths and plant remains. J. Hum. Evol. 63, 342–350. https://doi.org/10.1016/j.jhevol.2011.05.010.

Albert, R.M., Bamford, M.K., Stanistreet, I., Stollhofen, H., Rivera-Rondon, D., Rodriguez-Cintas, A., 2015. Vegetation landscape at DK locality, Olduvai Gorge, Tanzania. Palaeogeogr. Palaeoclimatol. Palaeoecol. 426, 34–45. https://doi.org/10.1016/j.palaeo.2015.02.022.

Albert, R.M., Bamford, M.K., Stanistreet, I.G., Stollhofen, H., Rivera-Rondon, C.A., Njau, J.K., Blumenschine, R.J., 2018. River-fed wetland palaeovegetation and palaeoecology at the HWK W site, Bed I, Olduvai Gorge. Rev. Palaeobot. Palynol. 259, 223–241. https://doi.org/10.1016/j.revpalbo.2018.09.010.

Antón, S.C., Potts, R., Aiello, L.C., 2014. Evolution of early *Homo*: an integrated biological perspective. Science 345 (6192), 1236828. https://doi.org/10.1126/science.1236828.

Araie, H., Nakamura, H., Toney, J.L., Haig, H.A., Plancq, J., Shiratori, T., Leavitt, P.R., Seki, O., Ishida, K., Sawada, K., Suzuki, I., Shiraiwa, Y., 2018. Novel alkenone-producing strains of genus Isochrysis (Haptophyta) isolated from Canadian saline lakes

show temperature sensitivity of alkenones and alkenoates. Org. Geochem. 121, 89–103. https://doi.org/10.1016/j.orggeochem.2018.04.008.
Aramendi, J., Uribelarrea, D., Arriaza, M.C., Arraiz, H., Barboin, D., Yraveda, J., Ortega, M.C., Gidna, A., Mabulla, A., Baquedano, E., Dominguez-Rodrigo, M., 2017. The paleoecology and taphonomy of AMK (Bed I, Olduvai Gorge) and its contributions to the understanding of the "Zinj" paleolandscape. Palaeogeogr. Palaeoclimatol. Palaeoecol. 488, 35–49. https://doi.org/10.1016/j.palaeo.2017.02.036.
Arráiz, H., Barboni, D., Ashley, G.M., Mabulla, A., Baquedano, E., Dominguez-Rodrigo, M., 2017. The FLK Zinj paleolandscape: Reconstruction of a 1.84 Ma wooded habitat in the FLK Zinj-AMK-PTK-DS archaeological complex, Middle Bed I (Olduvai Gorge, Tanzania). Palaeogeogr. Palaeoclimatol. Palaeoecol. 488, 9–20. https://doi.org/10.1016/j.palaeo.2017.04.025.
Ashley, G.M., 2007. Orbital rhythms, monsoons, and playa lake response, Olduvai Basin equatorial East Africa (ca. 1.85–1.74 Ma). Geology 35, 1091–1094. https://doi.org/10.1130/G24163A.1.
Ashley, G.M., Barboni, D., Dominguez-Rodrigo, M., Bunn, H.T., Mabulla, A.Z., Diez-Martin, F., Barba, R., Baquedano, E., 2010a. Paleoenvironmental and paleoecological reconstruction of a freshwater oasis in savannah grassland at FLK North, Olduvai Gorge, Tanzania. Quat. Res. 74, 333–343. https://doi.org/10.1016/j.yqres.2010.08.006.
Ashley, G.M., Barboni, D., Dominguez-Rodrigo, M., Bunn, H.T., Mabulla, A.Z.P., Diez-Martin, F., Barba, R., Baquwdano, E., 2010b. A spring and wooded habitat at FLK Zinj and their relevance to origins of human behavior. Quat. Res. 74 (3), 304–314. https://doi.org/10.1016/j.yqres.2010.07.015.
Ashley, G.M., de Wet, C.B., Barboni, D., Magill, C.R., 2016. Subtle signatures of seeps: Record of groundwater in a Dryland, DK, Olduvai Gorge, Tanzania. The Depositional Record 2, 4–21. https://doi.org/10.1002/dep2.11.
Ashley, G.M., Hay, R.L., 2002. Sedimentation patterns in a Plio-Pleistocene volcaniclastic rift-platform basin, Olduvai Gorge, Tanzania. Society for Sedimentary Geology, Special Publication 73. Tulsa, OK. https://doi.org/10.2110/pec.02.73.0107.
Bamford, M.K., Stanistreet, I.G., Stollhofen, H., Albert, R.M., 2008. Late Pliocene grassland from Olduvai Gorge, Tanzania. Palaeogeogr. Palaeoclimatol. Palaeoecol. 257, 280–293. https://doi.org/10.1016/j.palaeo.2007.09.003.
Barboni, D., Ashley, G.M., Dominguez-Rodrigo, M., Bunn, H.T., Mabulla, A.Z.P., Baquedano, E., 2010. Phytoliths infer locally dense and heterogeneous paleovegetation at FLK North and surrounding localities during upper Bed I time, Olduvai Gorge, Tanzania. Quat. Res. 74, 344–354. https://doi.org/10.1016/j.yqres.2010.09.005.
Bennett, C.E., Marshall, J.D., Stanistreet, I.G., 2012. Carbonate horizons, paleosols, and lake flooding cycles: Beds I and II of Olduvai Gorge, Tanzania. J. Hum. Evol. 63, 328–341. https://doi.org/10.1016/j.jhevol.2011.12.00.
Beverly, E.J., Ashley, G.M., Driese, S.G., 2014. Reconstruction of a Pleistocene paleocatena using micromorphology and geochemistry of lake margin paleo-Vertisols, Olduvai Gorge, Tanzania. Quat. Int. 322–323, 78–94. https://doi.org/10.1016/j.quaint.2013.10.005.
Blumenschine, R.J., 1995. Percussion marks, tooth marks, and experimental determinations of the timing of hominid and carnivore access to long bones at FLK *Zinjanthropus*, Olduvai Gorge, Tanzania. J. Hum. Evol. 29, 21–51. https://doi.org/10.1016/jhev.1995.1046.
Blumenschine, R.J., Masao, F.T., Stollhofen, H., Stanistreet, I.G., Bamford, M.K., Albert, R.M., Njau, J.K., Passack, K.A., 2012. Landscape distribution of Oldowan stone artifact assemblages across the fault compartments of the eastern Olduvai Lake Basin during lowermost Bed II times. J. Hum. Evol. 63 (384–394). https://doi.org/10.1016/j.jhevol.2011.05.003.
Blumenschine, R.J., Stanistreet, I.G., Njau, J.K., Bamford, M.K., Masao, F.T., Albert, R.M., Fernandez-Jalvo, Y., 2012. Environments and hominin activities across the FLK Peninsula during *Zinjanthropus* times (1.84 Ma), Olduvai Gorge, Tanzania. J. Hum. Evol. 63 (2), 364–383. https://doi.org/10.1016/j.jhevol.2011.10.001.
Bobe, R., Carvalho, S., 2019. The decline of Africa's largest mammals. Science 362, 892–893. https://doi.org/10.1126/science.aav6883.
Bohlin, L., Sjöstrand, U., Sodano, G., Djerassi, C., 1982. Sterols in marine invertebrates. 33. Structures of five new 3β-(hydroxymethyl)-A-norsteranes: indirect evidence for transformation of dietary precursors in sponges. J. Org. Chem. 47, 5309–5314. https://doi.org/10.1021/jo00148a016.
Bourbonniere, R.A., Meyers, P.A., 1996. Sedimentary geolipid records of historical changes in the watersheds and productivities of Lakes Ontario and Erie. Limnol. Oceanogr. 41, 352–359. https://doi.org/10.4319/lo.1996.41.2.0352.
Brassell, S.C., Eglinton, G., 1983. The potential of organic geochemical compounds as sedimentary indicators of upwelling. In: In Coastal Upwelling, Its Sediment Record, Part A (Suess E., Thiede J., eds.), pp. 545-571. Springer, Boston, MA. Springer, Boston, MA, pp. 545–571. doi:10.1007/978-1-4615-6651-9_27.
Brassell, S.C., Eglinton, G., 1984. Lipid indicators of microbial activity in marine sediments. In: In Heterotrophic Activity in the Sea (Hobbie, J.E., Williams, P.J.leB., eds.). pp. 481-503. Springer, Boston, MA. doi:10.1007/978-1-4684-9010-7_21.
Brassell, S.C., Eglinton, G., Maxwell, J.R., Philp, R.P., 1978. Natural background of alkanes in the aquatic environment. In: Hutzinger, O., van Lelyveld, L.H., Zoeteman, B.C.J. (Eds.), Aquatic Pollutants: Transformation and Biological Effects. Pergamon, Oxford, pp. 69–86. https://doi.org/10.1016/B978-0-08-022059-8.50010-8.
Brassell, S.C., Comet, P.A., Eglinton, G., Isaacson, P.J., McEvoy, J., Maxwell, J.R., Thomson, I.D., Tibbetts, P.J.C., Volkman, J.K., 1980. The origin and fate of lipids in the Japan Trench. In: Douglas, A.G., Maxwell, J.R. (Eds.), Advances in Organic Geochemistry 1979. Pergamon, Oxford, pp. 375–391. https://doi.org/10.1016/0079-1946(79)90120-4.
Brassell, S.C., Wardroper, A.M.K., Thomson, I.D., Maxwell, J.R., Eglinton, G., 1981. Specific acyclic isoprenoids as biological markers of methanogenic bacteria in marine sediments. Nature 290 (5808), 693. https://doi.org/10.1038/290693a0.
Brassell, S.C., Eglinton, G., Maxwell, J.R., 1983. The geochemistry of terpenoids and steroids. Biochem. Soc. Trans. 11, 575–586. https://doi.org/10.1042/bst0110575.
Brassell, S.C., Eglinton, G., Marlowe, I.T., Pflaumann, U., Sarnthein, M., 1986. Molecular stratigraphy: a new tool for climatic assessment. Nature 320, 129–133. https://doi.org/10.1038/320129a0.
Bunn, H.T., Kroll, E.M., Ambrose, S.H., Behrensmeyer, A.K., Binford, L.R., Blumenschine, R.J., Klein, R.G., McHenry, H.M., O'Brien, C.J., Wymer, J.J., 1986. Systematic butchery by Plio/Pleistocene hominids at Olduvai Gorge [and comments and reply]. Curr. Anthropol. 27 (5), 431–452. https://doi.org/10.1086/203467.
Bush, R.T., McInerney, F.A., 2013. Leaf wax *n*-alkane distributions in and across modern plants: Implications for paleoecology and chemotaxonomy. Geochim. Cosmochim. Acta 117, 161–179. https://doi.org/10.1016/j.gca.2013.04.016.
Canuel, E.A., Martens, C.S., 1996. Reactivity of recently deposited organic matter: degradation of lipid compounds near the sediment-water interface. Geochim. Cosmichim. Acta 60, 1793–1806. https://doi.org/10.1016/0016-7073(96)00045-2.
Castañeda, I.S., Schouten, S., 2011. A review of molecular organic proxies for examining modern and ancient lacustrine environments. Quat. Sci. Rev. 30, 2851–2891. https://doi.org/10.1016/j.quascirev.2011.07.009.
Cerling, T.E., Mbua, E., Kirera, F.M., Kyalo, F., Grine, F.E., Leakey, M.G., Sponheimer, M., Uno, K.T., 2011. Diet of Paranthropus boisei in the early Pleistocene of East Africa. Proc. Nat. Acad. Sci. 108, 9337–9347. https://doi.org/10.1073/pnas.1104627108.
Chikaraishi, Y., Naraoka, H., 2003. Compound-specific δD–δ^{13}C analyses of *n*-alkanes extracted from terrestrial and aquatic plants. Phytochem. 63, 361–371. https://doi.org/10.1016/S0031-9422(02)00749-5.
Colcord, D.E., Shilling, A.M., Sauer, P.E., Freeman, K.H., Njau, J.K., Stanistreet, I.G., Stollhofen, H., Schick, K.D., Toth, N., Brassell, S.C., 2018. Sub-Milankovitch paleoclimatic and paleoenvironmental variability in East Africa recorded by Pleistocene lacustrine sediments from Olduvai Gorge, Tanzania. Palaeogeogr. Palaeoclimatol. Palaeoecol. 495, 284–291. https://doi.org/10.1016/j.palaeo.2018.01.023.
Colcord, D.E., Shilling, A.M., Freeman, K.H., Njau, J.K., Stanistreet, I.G., Stollhofen, H., Schick, K.D., Toth, N., Brassell, S.C., 2019. Aquatic biomarkers record Pleistocene environmental changes at Paleolake Olduvai, Tanzania. Palaeogeog, Palaeoclim, Palaeoecol. 524, 250–261. https://doi.org/10.1016/j.palaeo.2019.04.001.
Coolen, M.J.L., Muyzer, G., Rijpstra, W.I.C., Schouten, S., Volkman, J.K., Sinninghe Damsté, J.S., 2004. Combined DNA and lipid analyses of sediments reveal changes in Holocene haptophyte and diatom populations in an Antarctic lake. Earth Planet. Sci. Lett. 223, 225–239. https://doi.org/10.1016/j.epsl.2004.04.014.
Cornford, C., Rullkötter, J., Welte, D., 1979. Organic geochemistry of DSDP Leg 47A, Site 397 eastern North Atlantic: organic petrography and extractable hydrocarbons. Init. Repts. Deep Sea Drill. Proj. 47 (Pt. 1), 419–432. https://doi.org/10.2973/dsdp.proc.47-1.120.1979.
Cranwell, P.A., Eglinton, G., Robinson, N., 1987. Lipids of aquatic organisms as potential contributors to lacustrine sediments-II. Org. Geochem. 11, 513–527. https://doi.org/10.1016/0146-6380(87)90007-6.
D'Andrea, W.J., Theroux, S., Bradley, R.S., Huang, X., 2016. Does phylogeny control U^{K}_{37}-temperature sensitivity? Implications for lacustrine alkenone paleothermometry. Geochim. Cosmochim. Acta 175, 168–180. https://doi.org/10.1016/j.gca.2015.10.031.
Dansgaard, W., Johnsen, S.J., Møller, J., Langway, C.C., 1969. One thousand centuries of climatic record from Camp Century on the Greenland Ice Sheet. Science 166, 377–380. https://doi.org/10.1126/science.166.3903.377.
Dansgaard, W., White, J., Johnsen, S., 1989. The abrupt termination of the Younger Dryas climate event. Nature 339, 532–534. https://doi.org/10.1038/339532a0.
Dart, R., 1925. *Australopithecus africanus* the man-ape of South Africa. Nature 115, 195–199. https://doi.org/10.1038/115195a0.
Deino, A.L., 2012. ^{40}Ar/^{39}Ar dating of Bed I, Olduvai Gorge, Tanzania, and the chronology of early Pleistocene climate change. J. Hum. Evol. 63, 251–273. https://doi.org/10.1016/j.jhevol.2012.05.004.
Deino, A.L., Kingston, J.D., Glen, J.M., Edgar, A.K., Hill, A., 2006. Precessional forcing of lacustrine sedimentation in the late Cenozoic Chemeron Basin, Central Kenya Rift, and calibration of the Gauss/Matuyama boundary. Earth Planet. Sci. Lett. 247, 41–60. https://doi.org/10.1016/j.epsl.2006.04.009.
Deino, A.L., King, J., McHenry, L.J., Stanistreet, I.G., Stollhofen, H., Toth, N., Schick, K.D., Njau, J.K., 2020. Chronostratigraphy and Age Modeling of Pleistocene Drill Cores from the Olduvai Basin, Tanzania (Olduvai Gorge Coring Project). Palaeogeog, Palaeoclim, Palaeoecol. (this volume).
deMenocal, P.B., 1995. Plio-Pleistocene African climate. Science 270, 53–59. https://doi.org/10.1126/science.270.5233.53.
deMenocal, P.B., 2004. African climate change and faunal evolution during the Pliocene–Pleistocene. Earth Planet. Sci. Lett. 220, 3–24. https://doi.org/10.1016/S0012-821X(04)00003-2.
deMenocal, P.B., 2011. Climate and human evolution. Science 331, 540–542. https://doi.org/10.1126/science.1190683.
Deocampo, D.M., Berry, P.A., Beverly, E.J., Ashley, G.M., Jarrett, R.E., 2017. Whole-rock geochemistry tracks precessional control of Pleistocene lake salinity at Olduvai Gorge, Tanzania: a record of authigenic clays. Geology 45, 683–686. https://doi.org/10.1130/G38950.1.
Didyk, B.M., Simoneit, B.R.T., Brassell, S.C., Eglinton, G., 1978. Organic geochemical indicators of palaeoenvironmental conditions of sedimentation. Nature 272, 216–222. https://doi.org/10.1038/272216a0.
Dominguez-Rodrigo, M., Baquedano, E., Mabulla, A., Mercader, J., Egeland, C.P., 2017. Paleoecological reconstructions of the Bed I and Bed II lacustrine basins of Olduvai Gorge (Tanzania) and insights into early human behavior. Palaeogeogr. Palaeoclimatol. Palaeoecol. 488, 1–8. https://doi.org/10.1016/j.palaeo.2017.05.009.
Donges, J.F., Donner, R.V., Trauth, M.H., Marwan, N., Schellnhuber, H.-J., Kurths, J.,

2011. Nonlinear detection of paleoclimate-variability transitions possibly related to human evolution. Proc. Natl. Acad. Sci. 108, 20422–20427. https://doi.org/10.1073/pnas.1117052108.
Douglas, P.M.J., Pagani, M., Eglinton, T.I., Brenner, M., Hodell, D.A., Curtis, J.H., Ma, K.F., Breckenridge, A., 2014. Pre-aged plant waxes in tropical lake sediments and their influence on the chronology of molecular paleoclimate proxy records. Geochim. Cosmochim. Acta 141, 346–364. https://doi.org/10.1016/j.gca.2014.06.030.
Driese, S.G., Ashley, G.M., 2016. Paleoenvironmental reconstruction of a paleosol catena, the Zinj archeological level, Olduvai Gorge, Tanzania. Quat. Res. 85, 133–146. https://doi.org/10.1016/j.yqres.2015.10.007.
Dumitrescu, M., Brassell, S.C., 2005. Biogeochemical assessment of sources of organic matter and paleo-productivity during the Early Aptian oceanic anoxic event at Shatsky Rise, ODP Leg 198. Org. Geochem. 36, 1002–1022. https://doi.org/10.1016/j.orggeochem.2005.03.001.
Eglinton, G., Hamilton, R.J., 1963. The distribution of alkanes. In: Chemical Plant Taxonomy. Academic Press, pp. 187–217. https://doi.org/10.1016/B978-0-12-395540-1.50012-9.
Etourneau, J., Schneider, R., Blanz, T., Martinez, P., 2010. Intensification of the Walker and Hadley atmospheric circulations during the Pliocene–Pleistocene climate transition. Earth Planet. Sci. Lett. 297, 103–110. https://doi.org/10.1016/j.epsl.2010.06.010.
Farrimond, P., Eglinton, G., Brassell, S.C., 1986. Geolipids of black shales and claystones in Cretaceous and Jurassic sediment sequences from the North American Basin. In: Summerhayes, C.P., Shackleton, N.J. (Eds.), North Atlantic Palaeoceanography. Blackwell, Oxford, pp. 347–360. https://doi.org/10.1144/GSL.SP.1986.021.01.25.
Feakins, S.J., Sessions, A.L., 2010. Controls on the D/H ratios of plant leaf waxes in an arid ecosystem. Geochim. Cosmochim. Acta 74, 2128–2141. https://doi.org/10.1016/j.gca.2010.01.016.
Ferland, T.M., Colcord, D.E., Shilling, A.M., Brassell, S.C., Stanistreet, I.G., Stollhofen, H., Njau, J.K., Schick, K.D., Toth, N., Freeman, K.H., 2020. Biased preservation of Pleistocene climate variability from Olduvai Gorge, Tanzania. Palaeogeogr. Palaeoclimat., Palaeoecol this volume.
Ficken, K.J., Li, B., Swain, D., Eglinton, G., 2000. An *n*-alkane proxy for the sedimentary input of submerged/floating freshwater aquatic macrophytes. Org. Geochem. 31, 745–749. https://doi.org/10.1016/S0146-6380(00)00081-4.
Fourcans, A., de Oteyza, T.G., Wieland, A., Sole, A., Diestra, E., van Bleijswijk, J., Grimalt, J.O., Kuhl, M., Esteve, I., Muyzer, G., Caumette, P., Duran, R., 2004. Characterization of functional bacterial groups in a hypersaline microbial mat community (Salins-de-Giraud, Camargue, France). FEMS Microbial Ecol. 51, 55–70. https://doi.org/10.1016/j.femsec.2004.07.012.
Gelpi, E., Schneider, H., Mann, J., Oró, J., 1970. Hydrocarbons of geochemical significance in microscopic algae. Phytochem. 9, 603–612. https://doi.org/10.1016/S0031-9422(00)85700-3.
van Grass, G., de Lange, F., de Leeuw, J.W., Schenck, P.A., 1982. A-nor-steranes, a novel class of sedimentary hydrocarbons. Nature 296, 59–61. https://doi.org/10.1038/296059a0.
Grossi, V., Hirschler, A., Raphel, D., Rontani, J.-F., de Leeuw, J.W., Bertrand, J.C., 1998. Biotransformation pathways of phytol in recent anoxic sediments. Org. Geochem. 29, 845–861. https://doi.org/10.1016/S0146-6380(98)00118-1.
Habermann, J.M., McHenry, L.J., Stollhofen, H., Tolosana-Delgado, R., Stanistreet, I.G., Deino, A.L., 2016. Discrimination, correlation, and provenance of Bed I tephrostratigraphic markers, Olduvai Gorge, Tanzania, based on multivariate analyses of phenocryst compositions. Sediment. Geol. 339, 115–133. https://doi.org/10.1016/j.sedgeo.2016.03.026.
Hanisch, S., Ariztegui, D., Püttmann, W., 2003. The biomarker record of Lake Albano, central Italy - Implications for Holocene aquatic system response to environmental change. Org. Geochem. 34, 1223–1235. https://doi.org/10.1016/S0146-6380(03)00118-9.
Hanisch, S., Wessels, M., Niessen, F., Schwalb, A., 2009. Late Quaternary lake response to climate change and anthropogenic impact: biomarker evidence from Lake Constance sediments. J. Paleolimnol. 41, 393–406. https://doi.org/10.1007/s10933-008-9232-4.
Hay, R.L., 1976. Geology of the Olduvai Gorge: A Study of Sedimentation in a Semiarid Basin. Univ of California Press.
Hay, R.L., Kyser, T.K., 2001. Chemical sedimentology and paleoenvironmental history of Lake Olduvai, a Pliocene lake in northern Tanzania. Geol. Soc. Amer. Bull. 113, 1505–1521. https://doi.org/10.1130/0016-7606(2001)113.
Hebting, Y., Schaeffer, P., Behrens, A., Adam, P., Schmitt, G., Schneckenburger, P., Bernasconi, S.M., Albrecht, P., 2006. Biomarker evidence for a major preservation pathway of sedimentary organic carbon. Science 312, 1627–1631. https://doi.org/10.1126/science.1126372.
Kennedy, J.A., Brassell, S.C., 1992. Molecular stratigraphy of the Santa Barbara basin: comparison with historical records of annual climate change. Org. Geochem. 19, 235–244. https://doi.org/10.1016/0146-6380(92)90040-5.
Leakey, M.D., 1969. Recent discoveries of hominid remains at Olduvai Gorge, Tanzania. Nature 223, 756. https://doi.org/10.1038/223756a0.
Leakey, M.D., 1971. Olduvai Gorge, Vol. 3: Excavations in Beds I and II, 1960–1963. Cambridge University Press (306 pp.).
Leakey, M.D., Clarke, R.J., Leakey, L.S., 1971. New hominid skull from Bed I, Olduvai Gorge, Tanzania. Nature 232, 308–312. https://doi.org/10.1038/232308a0.
Longman, M.W., Palmer, S.E., 1987. Organic geochemistry of mid-continent Middle and Late Ordovician oils. Am. Assoc. Petrol. Geol. Bull. 71, 938–950. https://doi.org/10.1306/948878F2-1704-11D7-8645000102C1865D.
Longo, W.M., Huang, Y., Yao, Y., Zhao, J., Giblin, A.E., Wang, X., Zech, R., Haberzettl, T., Jardillier, L., Toney, J., Liu, Zhonghui, Krivonogov, S., Kolpakova, M., Chu, G., D'Andrea, W., Harada, N., Nagashima, K., Sato, M., Yonenobu, H., Yamada, K., Gotanda, K., Shinozuka, Y., 2018. Widespread occurance of distinct alkenones from Group I haptophytes in freshwater lakes: Implications for paleotemperature and paleoenvironmental reconstructions. Earth Planet. Sci. Lett. 492, 239–250. https://doi.org/10.1016/j.epsl.2018.04.002.
Longo, W.M., Theroux, S., Giblin, A.E., Zheng, Y., James, T., Huang, Y., 2016. Temperature calibration and phylogenetically distinct distributions for freshwater alkenones: evidence from northern Alaskan lakes. Geochim. Cosmochim. Acta 180, 177–196. https://doi.org/10.1016/j.gca.2016.02.019.
Mackenzie, A.S., Brassell, S.C., Eglinton, G., Maxwell, J.R., 1982. Chemical fossils: the geological fate of steroids. Science 217, 491–504. https://doi.org/10.1126/science.217.4559.491.
Magill, C.R., Ashley, G.M., Freeman, K.H., 2013a. Ecosystem variability and early human habitats in eastern Africa. Proc. Natl. Acad. Sci. 110, 1167–1174. https://doi.org/10.1073/pnas.1206276110.
Magill, C.R., Ashley, G.M., Freeman, K.H., 2013b. Water, plants, and early human habitats in eastern Africa. Proc. Natl. Acad. Sci. 110, 1175–1180. https://doi.org/10.1073/pnas.1209405109.
Magill, C.R., Ashley, G.M., Dominguez-Rodrigo, M., Freeman, K.H., 2016. Dietary options and behavior suggested by plant biomarker evidence in an early human habitat. Proc. Natl. Acad. Sci. U. S. A. 113, 2874–2879. https://doi.org/10.1073/pnas.1507055113.
Marlowe, I.T., Green, J.C., Neal, A.C., Brassell, S.C., Eglinton, G., Course, P.A., 1984. Long chain (n-C_{37}-C_{39}) alkenones in the Prymnesiophyceae. Distribution of alkenones and other lipids and their taxonomic significance. Brit. Phycol. J. 19, 203–216. https://doi.org/10.1080/00071618400650221.
Maslin, M.A., Breirley, C.M., Milner, A.M., Shultz, S., Trauth, M.H., Wilson, K.E., 2014. East African climate pulses and early human evolution. Quat. Sci. Rev. 101, 1–17. https://doi.org/10.1016/j.quascirev.2014.06.012.
Maslin, MA, Christensen, B, 2007. Tectonics, orbital forcing, global climate change, and human evolution in Africa: introduction to the African paleoclimate special volume. J. Hum. Evol. 53, 443–464. https://doi.org/10.1016/j.jhevol.2007.06.005.
Maslin, M.A., Shultz, S., Trauth, M.H., 2015. A synthesis of the theories and concepts of early human evolution. Phil. Trans. R. Soc. B 370, 20140064. https://doi.org/10.1098/rstb.2014.0064.
Maxwell, S.J., Hopley, P.J., Upchurch, P., Soligo, S., 2018. Sporadic sampling, not climatic forcing, drives observed early hominin diversity. Proc. Natl. Acad. Sci. 115, 4891–4896. https://doi.org/10.1073/pnas.1721538115.
Mayewski, P.A., Meeker, L.D., Twickler, M.S., Whitlow, S., Yang, Q., Lyons, W.B., Prentice, M., 1997. Major features and forcing of high-latitude northern hemisphere atmospheric circulation using a 110,000- year-long glaciochemical series. J. Geophys. Res. 102, 26345–26366. https://doi.org/10.1029/96JC03365.
McClymont, E.L., Rosell-Melé, A., 2005. Links between the onset of modern Walker circulation and the mid-Pleistocene climate transition. Geology 33, 389–392. https://doi.org/10.1130/G21292.1.
McEvoy, J., Maxwell, J.R., 1983. Diagenesis of steroidal compounds in sediments from the Southern California Bight (DSDP Leg 63, Site 467). In: Bjorøy, M. (Ed.), Advances in Organic Geochemistry 1981. Wiley, Chichester, pp. 449–464.
McHenry, L.J., 2012. A revised stratigraphic framework for Olduvai Gorge Bed I based on tuff geochemistry. J. Hum. Evol. 63, 284–299. https://doi.org/10.1016/j.jhevol.2011.04.010.
McHenry, L.J., Kodikara, G.L.R., Stanistreet, I.G., Stollhofen, H, Njau, J.K., Schick, K., Toth, N., 2020b. Lake conditions and detrital sources of Paleolake Olduvai, Tanzania, reconstructed using X-ray Diffraction analysis of cores. Palaeogeog. Palaeoclimat. Palaeoecol. 109855.
McHenry, L.J., Stanistreet, I.G., Stollhofen, H., Njau, J., Toth, N., Schick, K., 2020a. Tuff fingerprinting and correlations between OGCP cores and outcrops for Pre-Bed I and Bed I/II at Olduvai Gorge, Tanzania. Palaeogeog. Palaeoclimat. Palaeoecol. 548, 109630. https://doi.org/10.1016/j.palaeo.2020.109630.
Meyers, P.A., 2003. Applications of organic geochemistry to paleolimnological reconstructions: a summary of examples from the Laurentian Great Lakes. Org. Geochem. 34, 261–289. https://doi.org/10.1016/S0146-6380(02)00168-7.
Meyers, P.A., Ishiwatari, R., 1993. Lacustrine organic geochemistry - an overview of indicators of organic matter sources and diagenesis in lake sediments. Org. Geochem. 20, 867–900. https://doi.org/10.1016/0146-6380(93)90100-P.
Mollel, G.F., Swisher, C.C., 2012. The Ngorongoro Volcanic Highland and its relationships to volcanic deposits at Olduvai Gorge and East African Rift volcanism. J. Hum. Evol. 63, 274–283. https://doi.org/10.1016/j.jhevol.2011.09.001.
Nagashima, K., Sato, M., Yonenobu, H., Yamada, K., Gotanda, K., Shinozuka, Y., 2018. Widespread occurrence of distinct alkenones from Group I haptophytes in freshwater lakes: Implications for paleotemperature and paleoenvironmental reconstructions. Earth Planet. Sci. Lett. 492, 239–250. https://doi.org/10.1016/j.epsl.2018.04.002.
Nakamura, H., Sawada, K., Araie, H., Suzuki, I., Shiraiwa, Y., 2014. Long chain alkenes, alkenones and alkenoates produced by the haptophyte alga *Chrysotila lamellosa* CCMP1307 isolated from a salt marsh. Org. Geochem. 66, 90–97. https://doi.org/10.1016/j.orggeochem.2013.11.007.
Nicholson, S.E., 2000. The nature of rainfall variability over Africa on time scales of decades to millenia. Glob. Planet. Chang. 26, 137–158. https://doi.org/10.1016/S0921-8181(00)00040-0.
Pearson, E.J., Juggins, S., Farrimond, P., 2008. Distribution and significance of long-chain alkenones as salinity and temperature indicators in Spanish saline lake sediments. Geochim. Cosmochim. Acta 72, 4035–4046. https://doi.org/10.1016/j.gca.2008.05.052.
Philp, R.P., Brown, S., Calvin, M., Brassell, S.C., Eglinton, G., 1978. Hydrocarbon and fatty acid distributions in recently deposited algal mats at Laguna Guerrero, Baja California. In: Krumbein, W.E. (Ed.), Environmental Biogeochemistry and Geomicrobiology: Vol. 1. The Aquatic Environment. Ann Arbor Science, Ann Arbor,

pp. 255–270.
Potts, R., 1984. Home bases and early hominids: reevaluation of the fossil record at Olduvai Gorge suggests that the concentrations of bones and stone tools do not represent fully formed campsites but an antecedent to them. Am. Scientist 72, 338–347.
Potts, R., 1998. Environmental hypotheses of hominin evolution. American journal of physical anthropology 107 (S27), 93–136. https://doi.org/10.1002/(SICI)1096-8644(1998)107:27+<93::AID-AJPA5>3.0.CO;2-X.
Potts, R., 2013. Hominin evolution in settings of strong environmental variability. Quat. Sci. Rev. 73, 1–13. https://doi.org/10.1016/j.quascirev.2013.04.003.
Potts, R., Faith, J.T., 2015. Alternating high and low climate variability: the context of natural selection and speciation in Plio-Pleistocene hominin evolution. J. Hum. Evol. 87, 5–20. https://doi.org/10.1016/j.jhevol.2015.06.014.
Prahl, F.G., Muehlhausen, L.A., Zahnle, D.L., 1988. Further evaluation of long-chain alkenones as indicators of paleoceanographic conditions. Geochim. Cosmochim. Acta 52, 2303–2310. https://doi.org/10.1016/0016-7037(88)90132-9.
Pu, Y., Wang, C., Meyers, P.A., 2017. Origins of biomarker aliphatic hydrocarbons in sediments of alpine Lake Ximencuo, China. Palaeogeog. Palaeoclimatol. Palaeoecol. 475, 106–114. https://doi.org/10.1016/j.palaeo.2017.03.011.
Pu, Y., Jia, J., Cao, J., 2018. The aliphatic hydrocarbon distributions of terrestrial plants around an alpine lake: a pilot study from Lake Ximencuo. Eastern Qinghai-Tibet Plateau. Front. Earth Sci. 12, 600–610. https://doi.org/10.1007/s11707-017-0685-5.
Rampen, S.W., Abbas, B.A., Schouten, S., Sinninghe Damsté, J.S., 2010. A comprehensive study of sterols in marine diatoms (Bacillariophyta): implications for their use as tracers for diatom productivity. Limnol. Oceanogr. 55, 91–105. https://doi.org/10.4319/lo.2010.55.1.0091.
Randlett, M.-E., Coolen, M.J.L., Stockhecke, M., Pickarski, N., Litt, T., Balkema, C., Kwiecien, O., Tomonaga, Y., Wehrli, B., Schubert, C.J., 2014. Alkenone distribution in Lake Van sediment over the last 270 ka: influence of temperature and haptophyte species composition. Quat. Sci. Rev. 104, 53–62. https://doi.org/10.1016/j.quascirev.2014.07.009.
Ravelo, A.C., 2006. Walker circulation and global warming: Lessons from the geologic past. Oceanogr. 19 (4), 114–122. https://doi.org/10.5670/oceanog.2006.10.
Ravelo, A.C., Andreasen, D.H., Lyle, M., Olivarez, L.A., Wara, M.W., 2004. Regional climate shifts caused by gradual global cooling in the Pliocene epoch. Nature 429, 263–267. https://doi.org/10.1038/nature02567.
Raymo, M.E., Ganley, K., Carter, S., Oppo, D.W., McManus, J., 1998. Millennial-scale climate instability during the early Pleistocene epoch. Nature 392, 699–702. https://doi.org/10.1038/33658.
Reti, J.S., 2016. Quantifying Oldowan stone tool production at Olduvai Gorge, Tanzania. Plos One 11 (1), e0147352. https://doi.org/10.1371/journal.pone.0147352.
Rontani, J.-F., Bonin, P., 2011. Production of pristane and phytane in the marine environment: role of prokaryotes. Res. Microbiol. 162, 923–933. https://doi.org/10.1016/j.resmic.2011.01.012.
Sachse, D., Radke, J., Gleixner, G., 2004. Hydrogen isotope ratios of recent lacustrine sedimentary n-alkanes record modern climate variability. Geochim. Cosmochim. Acta 68, 4877–4889. https://doi.org/10.1016/j.gca.2004.06.004.
Schouten, S., Rijpstra, W.I.C., Kok, M., Hopmans, E.C., Summons, R.E., Volkman, J.K., Sinninghe Damsté, J.S., 2001. Molecular organic tracers of biogeochemical processes in a saline meromictic lake (Ace Lake), Org. Geochem 65, 1629–1640. https://doi.org/10.1016/S0016-7037(00)00627-X.
Schouten, S., Middelburg, J.J., Hopmans, E.C., Sinninghe Damsté, J.S., 2010. Fossilization and degradation of intact polar lipids in deep subsurface sediments: a theoretical approach. Geochim. Cosmochim. Acta 74, 3806–3814. https://doi.org/10.1016/j.gca.2010.03.029.
Seki, O., Nakatsuka, T., Shibata, H., Kawamura, K., 2010. A compound-specific *n*-alkane $\delta^{13}C$ and δD approach for assessing source and delivery processes of terrestrial organic matter within a forested watershed in northern Japan. Geochim. Cosmochim. Acta 74, 599–613. https://doi.org/10.1016/j.gca.2009.10.025.
Shilling, A.S., Colcord, D.E., Karty, J., Hansen, A., Freeman, K.H., Njau, J.K., Stanistreet, I.G., Stollhofen, H., Schick, K.D., Toth, N., Brassell, S.C., 2019. Biomarker evidence for environmental changes of Pleistocene Lake Olduvai during the transitional sequence of OGCP core 2A that encompasses Tuff IB (~1.848 Ma). Palaeogeogr. Palaeoclimatol. Palaeoecol. 532, 109267. https://doi.org/10.1016/j.palaeo.2019.109267.
Shultz, S., Maslin, M., 2013. Early human speciation, brain expansion and dispersal influenced by African climate pulses. PLoS One 8, e76750. https://doi.org/10.1371/journal.pone.0076750.
Shultz, S., Nelson, E., Dunbar, R.I., 2012. Hominin cognitive evolution: identifying patterns and processes in the fossil and archaeological record. Phil. Trans. Royal Soc. B: Biol. Sci. 367, 2130–2140. https://doi.org/10.1098/rstb.2012.0115.
Sikes, N.E., Ashley, G.M., 2007. Stable isotopes of pedogenic carbonates as indicators of paleoecology in the Plio-Pleistocene (upper Bed I), western margin of the Olduvai Basin, Tanzania. J. Hum. Evol. 53, 574–594. https://doi.org/10.1016/j.jhevol.2006.12.008.
Sinninghe Damsté, J.S., Kock-van Dalen, A.C., De Leeuw, J.W., Schenck, P.A., Sheng, G., Brassell, S.C., 1987. The identification of mono-, di-and trimethyl 2-methyl-2-(4,8,12-trimethyltridecyl)chromans and their occurrence in the geosphere. Geochim. Cosmochim. Acta 51, 2393–2400. https://doi.org/10.1016/0016-7037(87)90292-4.
Sirocko, F., Garbe-Schönberg, D., McIntyre, A., Molfino, B., 1996. Teleconnections between the subtropical monsoons and high-latitude climates during the last deglaciation. Science 272, 526–529. https://doi.org/10.1126/science.272.5261.526.
Speth, J.D., Davis, D.D., 1976. Seasonal variability in early hominid predation. Science 192, 441–445. https://doi.org/10.1126/science.192.4238.441.
Stanistreet, I.G., 2012. Fine resolution of early hominin time, Beds I and II, Olduvai Gorge, Tanzania. J. Hum. Evol. 63, 300–308. https://doi.org/10.1016/j.jhevol.2012.03.001.
Stanistreet, I.G., Stollhofen, H., Njau, J.K., Farrugia, P., Pante, M.C., Masao, F.T., Albert, R.M., Bamford, M.K., 2018a. Lahar inundated, modified and preserved 1.88 Ma early hominin (OH24 and OH56) Olduvai DK site. J. Hum. Evol. 116, 27–42. https://doi.org/10.1016/j.jhevol.2017.11.011.
Stanistreet, I.G., McHenry, L.J., Stollhofen, H., de la Torre, I., 2018b. Sequence stratigraphic context of EF-HR and HWK EE archaeological sites, and the Oldowan/Acheulean succession at Olduvai Gorge, Tanzania. J. Hum. Evol. 120, 19–31. https://doi.org/10.1016/j.jhevol.2018.01.005.
Stanistreet, I.G., Stollhofen, H., Deino, A., McHenry, L., Toth, N., Schick, K., Njau, J., 2020a. New Olduvai Basin stratigraphy and stratigraphic concepts revealed by OGCP cores into the Palaeolake Olduvai depocentre, Tanzania. Palaeogeogr. Palaeoclimatol. Palaeoecol (this volume).
Stanistreet, I.G., Boyle, J.F., Stollhofen, H., Deocampo, D.M., Deino, A., McHenry, L.J., Toth, N., Schick, K., Njau, J.K., 2020b. Palaeosalinity and palaeoclimatic geochemical proxies (elements Ti, Mg, Al) vary with Milankovitch cyclicity (1.3 to 2.0 Ma), OGCP cores, Palaeolake Olduvai, Tanzania. Palaeogeogr. Palaeoclimatol. Palaeoecol. https://doi.org/10.1016/j.palaeo.2020.109656.
Stollhofen, H., Stanistreet, I.G., McHenry, L.J., Mollel, G.F., Blumenschine, R.J., Masao, F.T., 2008. Fingerprinting facies of the Tuff IF marker, with implications for early hominin palaeoecology, Olduvai Gorge, Tanzania. Palaeogeogr. Palaeoclimatol. Palaeoecol. 259, 382–409. https://doi.org/10.1016/j.palaep.2007.09.024.
Theroux, S., D'Andrea, W.J., Toney, J., Amaral-Zettler, L., Huang, Y., 2010. Phylogenetic diversity and evolutionary relatedness of alkenone-producing haptophyte algae in lakes: Implications for continental paleotemperature reconstructions. Earth Planet. Sci. Lett. 300, 311–320. https://doi.org/10.1016/j.epsl.2010.10.009.
Toney, J.L., Theroux, S., Andersen, R.A., Coleman, A., Amaral-Zettler, L., Huang, Y., 2012. Culturing of the first 37:4 predominant lacustrine haptophyte: geochemical, biochemical, and genetic implications. Geochim. Cosmochim. Acta 78, 51–64. https://doi.org/10.1016/j.gca.2011.11.024.
Trauth, M.H., Maslin, M.A., Deino, A.L., Strecker, M.R., 2005. Late Cenozoic moisture history or East Africa. Science 309, 2051–2053. https://doi.org/10.1126/science.1112964.
Trauth, M.H., Maslin, M.A., Deino, A.L., Strecker, M.R., Bergner, A.G., Duhnforth, M., 2007. High- and low- latitude forcing of Plio-Pleistocene East African climate and human evolution. J. Hum. Evol. 53, 475–486. https://doi.org/10.1016/j.jhevol.206.12.009.
Trauth, M.H., Maslin, M.A., Deino, A.L., Junginger, A., Lesoloyia, M., Odada, E.O., Olago, D.O., Olaka, L.A., Strecker, M.R., Tiedemann, R., 2010. Human evolution in a variable environment: the amplifier lakes of Eastern Africa. Quat. Sci. Rev. 29, 2981–2988. https://doi.org/10.1016/j.quascirev.2010.07.007.
Volkman, J.K., 1988. Biological marker compounds as indicators of the depositional environments of petroleum source rocks. Geol. Soc. London, Special Publ. 40, 103–122. https://doi.org/10.1144/GSL.SP.1988.040.01.10.
Volkman, J.K., 2003. Sterols in microorganisms. Appl. Microbiol. Biotechnol. 60, 495–506. https://doi.org/10.1007/s00253-002-1172-8.
Volkman, J.K., Allen, D.I., Stevenson, P.L., Burton, H.R., 1986. Bacterial and algal hydrocarbons in sediments from a saline Antarctic lake, Ace Lake. Org. Geochem. 10, 671–681. https://doi.org/10.1016/S0146-6380(86)80003-1.
Vrba, E.S., 1995. On the connections between paleoclimate and evolution. In: Vrba, E.S., Denton, G.H., Partridge, T.C., Burckle, L.H. (Eds.), Paleoclimate and Evolution with Emphasis on Human Origins. Yale University Press, New Haven, pp. 24–45.
Ward, D.M., 2006. Microbial diversity in natural environments: focusing on fundamental questions. Antonie Van Leeuwenhoek 90, 309–324. https://doi.org/10.1007/s10482-006-9090-x.
Weirauch, D., Billups, K., Martin, P., 2008. Evolution of millennial-scale climate variability during the mid-Pleistocene. Paleoceanogr. 23, PA3216. https://doi.org/10.1029/2007PA001584.
Wu, M.S., West, A.J., Feakins, S.J., 2019. Tropical soil profiles reveal the fate of plant wax biomarkers during soil storage. Org. Geochem. 128, 1–13. https://doi.org/10.1016/j.orggeochem.2018.12.011.
Wynn, J.G., Bird, M.I., 2007. C4-derived soil organic carbon decomposes faster than its C3 counterpart in mixed C3/C4 soils. Glob. Chang. Biol. 13, 2206–2217. https://doi.org/10.1111/j.1365-2486.2007.01435.x.
Zhang, Z., Metzger, P., Sachs, J.P., 2011. Co-occurrence of long chain diols, keto-ols, hydroxy acids and keto acids in recent sediments of Lake El Junco, Galápagos Islands. Org. Geochem. 42 (7), 823–837. https://doi.org/10.1016/j.orggeochem.2011.04.012.
Zhang, Y.G., Pagani, M., Liu, Z., 2014. A 12-million-year temperature history of the tropical Pacific Ocean. Science 344, 84–87. https://doi.org/10.1126/science.1246172.